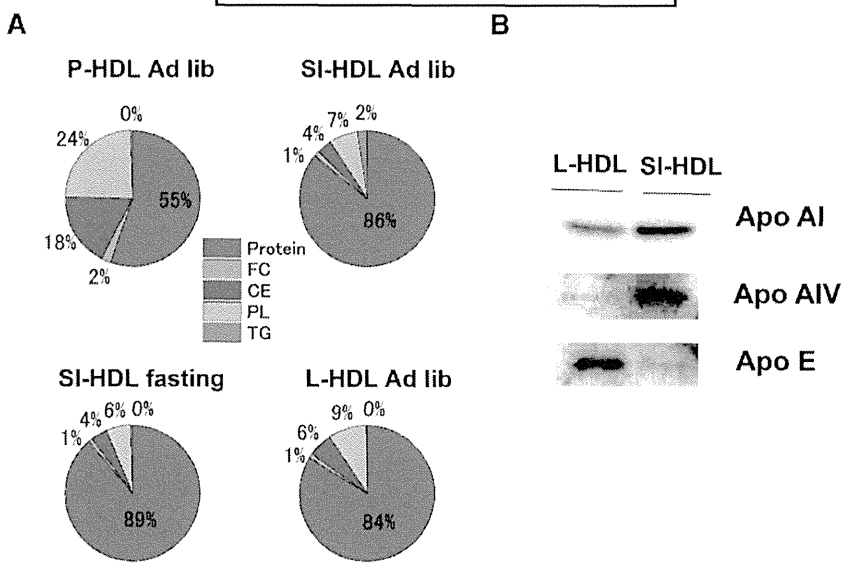

Fig. 4. Lipid and apo composition of HDL in SI lymph perfusates from WT mice. A: Lipid and protein composition of HDL in plasma (P-HDL), SI lymph perfusates (SI-HDL), and liver perfusates (L-HDL) separated by serial preparative ultracentrifugation. HDL was further separated by HPLC to determine its lipid composition. B: Comparison of apo compositions of SI-HDL and L-HDL. SI-HDL and L-HDL were obtained by in situ perfusion followed by serial preparative ultracentrifugation and subjected to SDS-PAGE followed by Western blot analysis using antibodies against the indicated apos.

Apo composition of SI-HDL

To characterize the apo composition of SI-HDL, L-HDL and SI-HDL separated by ultracentrifugation from liver perfusates and SI lymph perfusates, respectively, were run on SDS-PAGE and then subjected to Western blot analysis for apo AI, apo AIV, and apo E (Fig. 4B). As shown in Fig. 4B, L-HDL contained a very limited amount of apo AIV but a considerable amount of apo E, whereas an opposite trend was seen for SI-HDL. This result indicates that SI-HDL was rich in apo AIV compared with L-HDL, and SI-HDL is different from L-HDL with respect to the composition of apos.

Size distribution of SI-HDL

Because SI-HDL was protein rich compared with P-HDL (Table 1), we used EM to examine the size distribution of HDL separated using ultracentrifugation from SI lymph perfusates and plasma of WT mice (**Fig. 5**). Fig. 5A shows the representative negative-stain electron micrographs of SI-HDL and P-HDL. As shown, SI-HDL particles were a population of spheres with a very small number of discs. We measured the particle diameter of spherical particles in SI-HDL and P-HDL (Fig. 5B, C). Fig. 5B shows the size distribution of SI-HDL and P-HDL. As shown, SI-HDL particles, similar to P-HDL, were heterogeneous in size, but the distribution of SI-HDL particles was more diverse than that of P-HDL, and the size distributions of SI-HDL and P-HDL overlaid (Fig. 5B). However, SI-HDL apparently had a higher proportion of smaller particles as compared with P-HDL (Fig. 5B). Fig. 5C shows the individual data and the box plots of SI-HDL and P-HDL. As shown, although the size range of SI-HDL covered that of P-HDL, the peak diameter of SI-HDL particles shifted toward smaller particles as compared with that of P-HDL, and the average size of SI-HDL particles (mean ± SD: 11.06 ± 2.70 nm) was significantly ($P < 0.001$) smaller than that of P-HDL particles (12.94 ± 1.64 nm). This result indicates that the particle size of SI-HDL was smaller than that of P-HDL.

Inhibitors of ABCA1 and LCAT affect the formation of SI-HDL

Because we have shown that most of the HDL particles secreted from the SI are spherical using EM (Fig. 5A), to identify the mechanism for SI-HDL assembly, we examined the effects of inhibitors of ABCA1 and LCAT on the formation of SI-HDL. It is well known that ABCA1 lipidates apo AI to form HDL and LCAT converts lipid-poor pre-β-migrating HDL to mature α-migrating HDL. We used glyburide (26) and DTNB (27) as inhibitors of ABCA1 and LCAT, respectively (**Fig. 6A**). The effects of ABCA1 and LCAT inhibitors were examined by collecting SI lymph perfusates from WT mice that underwent in situ perfusion using buffers with and without the presence of the inhibitors (Fig. 6).

As shown in Fig. 6B, nondenaturing PAGE followed by Western blot analysis for apo AI showed that there was a marked increase in free apo AI and small HDL in SI lymph perfusates in the presence of glyburide compared with the absence of glyburide. This result suggests that ABCA1 is involved in the lipidation of apo AI to form SI-HDL.

As shown in Fig. 6C, two-dimensional electrophoresis of SI lymph perfusates followed by Western blotting for apo AI showed that the presence of premature HDL such as pre-β1- and pre-β2-HDL (41, 42) was observed in the presence of DTNB, but not in the absence of DTNB. A reduction in α-HDL particle size was also observed in the

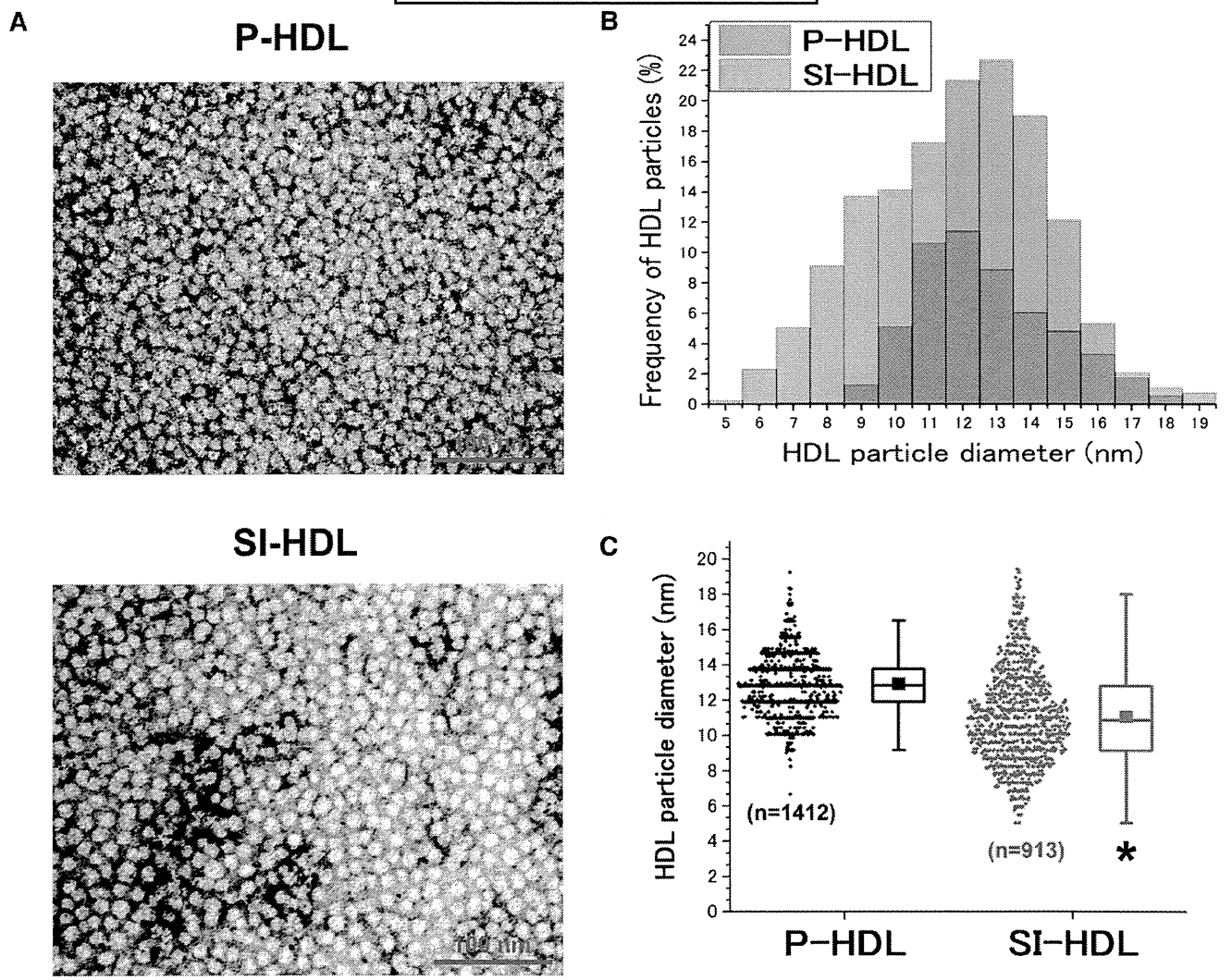

Fig. 5. Electron micrographs of negatively stained HDL from SI lymph perfusates. A: Representative negative-stain EM of HDL separated by serial ultracentrifugation from SI lymph perfusates (SI-HDL, lower panel) and plasma (P-HDL, upper panel). Magnification: 200,000×; scale bar: 100 nm. B: Size distribution of SI-HDL and P-HDL particles from negative-stain electron micrographs. The frequency distributions of the size of SI-HDL (pink bars; n = 913) and P-HDL (gray bars; n = 1,412) were plotted together, and the red bars represent the overlaid parts. Two measurements were made for the diameter of each HDL particle, and the mean diameter was used to calculate the size frequency. C: Box-and-whisker plots showing the mean (■), median (middle bar in the rectangle), and 10th (bottom bar), 25th (bottom of rectangle), 75th (top of rectangle), and 90th (top bar) percentiles of the sizes of SI-HDL (black) and P-HDL (red) particles. The individual data are shown on the left of the boxes. * $P < 0.001$, SI-HDL versus P-HDL, assessed by the Wilcoxon rank sum test.

presence of DTNB (Fig. 6C). This result suggests that LCAT may be involved in the maturation of SI-HDL.

Although our experiments were limited in that the inhibitory effects of ABCA1 and LCAT are unknown, our results suggest that ABCA1 and LCAT may play important parts in the formation of SI-HDL.

Nutritional regulation of the production of HDL from SI

A previous study showed that intestine significantly contributes to plasma HDL-C levels (44). We examined the effects of fasting and high-fat feeding on the production of HDL from SI in WT mice using our in situ perfusion model to clarify the nutritional regulation of SI-HDL. HDL in lymph perfusates collected under different nutritional conditions was analyzed by non-SDS-PAGE followed by Western blot analysis for apo AI. As shown in **Fig. 7A**, plasma HDL-C levels and the contents of HDL-apo AI in SI lymph perfusates from WT mice ad libitum were markedly reduced after 24 h fasting. In contrast, a 4-week high-fat diet markedly increased plasma HDL-C levels and the contents of HDL-apo AI in lymph perfusates from WT mice (Fig. 7B). These results indicate that fasting reduces and high-fat diet increases the production of HDL from the SI.

Apo E KO reduces the production of HDL from the SI

Apo E KO mice are characterized by a marked reduction of HDL-C levels in plasma. Because intestinal HDL has been shown to significantly contribute to plasma HDL (16), we used our in situ perfusion model to examine whether

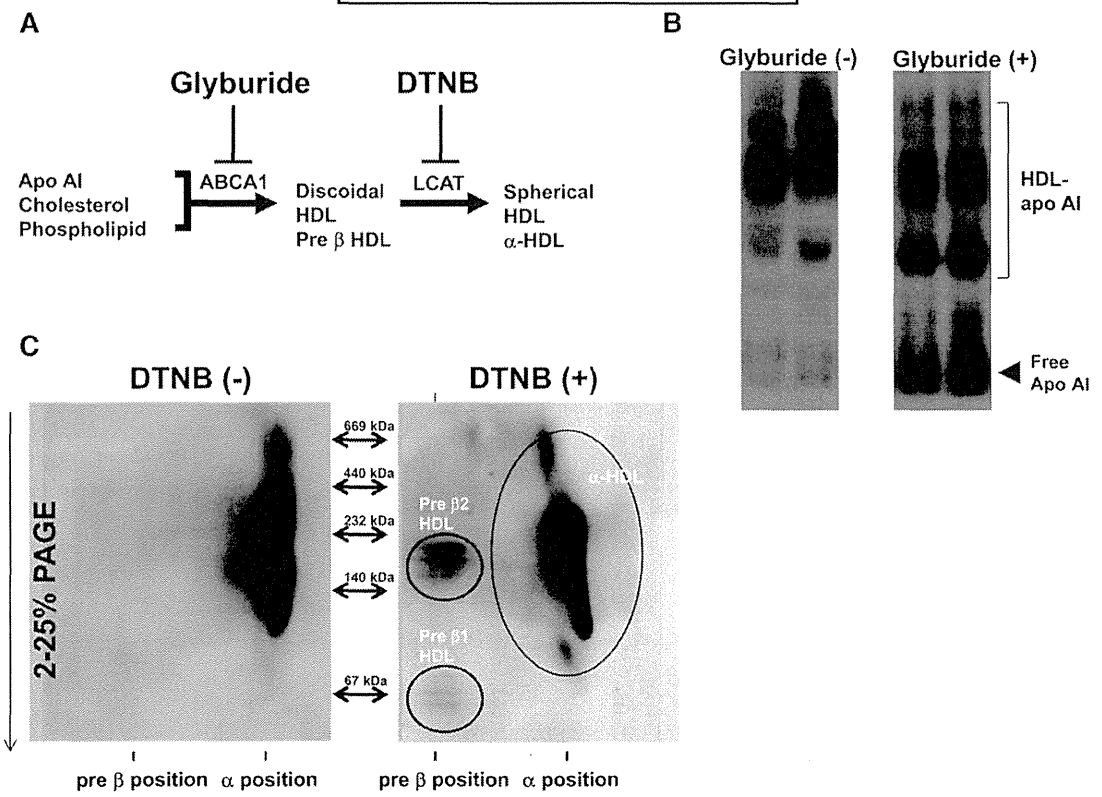

Fig. 6. Effects of glyburide and DTNB on the assembly of SI-HDL. A: Possible mechanism for the assembly of SI-HDL. Glyburide and DTNB are known inhibitors of ABCA1 and LCAT, respectively. B: Effect of glyburide on immunoblot patterns of HDL in SI lymph perfusates from WT mice. WT mice were subjected to in situ SI perfusion in the presence (right panel) and absence (left panel) of glyburide in the perfusion buffer. SI-HDL was run on non-SDS-PAGE followed by the detection of apo AI. Arrowhead represents free apo AI. C: Effect of DTNB on the formation of SI-HDL. SI lymph perfusates were obtained from WT mice that were perfused using a perfusion buffer in the presence (right panel) and absence (left panel) of DTNB in the perfusion buffer.

the production of HDL from the SI is reduced in apo E KO mice. As shown in Fig. 7C, apo E KO mice had markedly lower levels of HDL-C and reduced contents of HDL-apo AI in SI lymph perfusates as compared with WT mice. These results indicate that apo E may play a role in the biogenesis of SI-HDL.

DISCUSSION

To selectively evaluate HDL produced from the intestine, we developed an in situ perfusion model using surgically isolated mouse SI. Using our in situ perfusion model, we found that the SI produces HDL in mice and ABCA1 plays an important role in the production of SI-HDL, that SI-HDL is different from HDL produced by the liver, and that SI-HDL may be regulated by nutritional and genetic factors.

Our in situ perfusion model using surgically isolated mouse SI was developed for the selective evaluation of SI-HDL because HDL in mesenteric lymph collected from anesthetized mice originates either from the secretion by the SI or from the filtration from plasma through the blood capillary-lymph loop into the intestinal lymph duct (19–22).

Our novel in situ perfusion model achieves the selective evaluation of HDL by dissociating HDL production by the SI from the filtration of HDL from plasma. In this model, arterial blood supply for the SI is blocked by ligation of abdominal aorta and other arteries, leaving only the superior mesenteric artery open as the perfusion inlet (Fig. 1A). Perfusion buffer is pumped through a needle that is connected to a tube and inserted antegrade through the thoracic descending aorta into the abdominal aorta just before ligation of the abdominal aorta (Fig. 1A). Therefore, after perfusion starts, no additional systemic blood will enter the SI, and the possible filtration of plasma HDL from the systemic circulation into the SI lymph duct can be prevented. The SI lymph duct and portal vein are cannulated as outlets for perfusion buffer (Fig. 1A). Under these conditions, the HDL in the infusates collected from the SI lymph duct would originate only from the SI.

Using our in situ perfusion model, we found that HDL was detected in SI lymph perfusates from WT mice (Fig. 1B), indicating that the SI produces HDL. This finding supports the notion that the intestine, along with the liver, is an important site for the secretion of apo AI and the production of HDL (12–16). We did not detect HDL in SI lymph perfusates from ABCA1 mice (Fig. 1B), indicating that ABCA1 is essential for the production of HDL by the

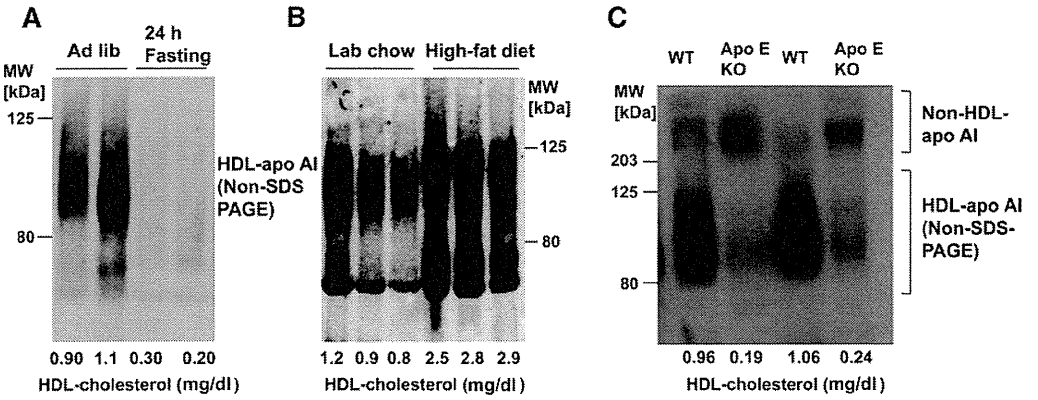

Fig. 7. Nutritional and genetic regulation of SI-HDL. The HDL-C concentration (mg/dl) in different perfusates was measured by HPLC as described in the Methods and is shown under each column. A: Effect of fasting on SI-HDL in WT mice. Mice were subjected to in situ perfusion at ad libitum and after 24 h of fasting. SI lymph perfusates were analyzed by using non-SDS-PAGE followed by Western blot analysis for apo AI. B: Effect of a high-fat diet on SI-HDL in WT mice. Mice were subjected to in situ SI perfusion after being fed a high-fat diet for 4 weeks. C: Comparison of SI-HDL production in 14-week-old WT and apo E KO mice.

SI. This finding supports those of Brunham et al. (16) that mice that specifically lack ABCA1 in the intestine had ~30% lower plasma HDL-C levels. However, we detected free apo AI in SI lymph perfusates from ABCA1 mice (Fig. 1B), indicating that cellular lipids are not available for the lipidation of apo AI to form SI-HDL in the absence of ABCA1 (45).

Because SI-HDL is not formed in the absence of ABCA1, we used ABCA1 KO mice to clarify whether plasma HDL can filtrate from the abdominal aorta through the SI into a lymph duct. We perfused the SI of ABCA1 KO mice using perfusion buffer to which had been added serum from WT mice and found that the collected SI lymph perfusates contained a substantial amount of HDL (Fig. 1C). It is possible that lipids in lipoproteins in the aortic perfusate may be delivered to the SI through transintestinal transport, that is, via the transintestinal cholesterol efflux pathway (48), and lipidate apo AI from intestinal secretion to form HDL. However, in the absence of ABCA1, which is located at the basolateral membrane of enterocytes (49), cellular lipids will not be available to free apo AI to form HDL. Therefore, HDL that was detected in SI lymph perfusates of ABCA1 mice perfused with serum from WT mice (Fig. 1C) can originate only from filtration of plasma HDL. Using our in situ perfusion model, we provided direct evidence that systemic plasma HDL can filtrate into the SI lymph duct.

One of the most likely mechanisms responsible for this perfusion is the "blood capillary-lymph loop" (50). Our finding that no apo B was present in SI lymph perfusates from ABCA1 KO mice that were perfused with buffer containing serum from WT mice indicated that HDL from the systemic circulation can, whereas apo-B-containing lipoproteins cannot, filter into the SI lymph duct (Fig. 1C), suggesting that bigger molecules cannot pass through the blood-capillary wall. Consistent with this finding, apo B48, but not apo B100, was detected in our analyses of apos in ultracentrifugation density fractions of lipoproteins in SI lymph perfusates from WT mice (Fig. 3B). Therefore, we consider the conventional cannulation experiment to be useful for the analysis of apo-B-containing lipoproteins because we used it to demonstrate an increase in the production of CMs in CD36 KO mice (51). However, for the selective evaluation of SI-HDL, the newly developed perfusion technique may be the best method available for eliminating the interference of plasma HDL.

Our finding that HDL was produced by the SI (Fig. 1A) but plasma HDL can also filtrate into the SI lymph duct (Fig. 1B) resolves controversies regarding intestinal-derived HDL (19–22). A previous study showed that HDL from the intestinal lymph duct obtained in vivo from anesthetized mice is likely to contain HDL from the systemic circulation, the majority of which is derived from the liver (16). Therefore, peptide mapping of HDL using LC/MS was performed to compare SI-HDL in SI lymph perfusates collected using our in situ perfusion model, C-HDL collected from the SI lymph duct in anesthetized mice, and L-HDL collected from liver perfusates (Fig. 2). C-HDL and L-HDL were very similar in that they had the same number of major peptides and relative peptide-ion intensities (Fig. 2C, D). This result agrees with the finding of Brunham et al. (16) that intestinal HDL in mice that lacked intestinal ABCA1 predominantly originates from the liver.

However, we found that SI-HDL in SI lymph perfusates was different from C-HDL and L-HDL in that SI-HDL contained additional major peptides (m/z 542 and m/z 524) that were not detected in L-HDL or C-HDL (Fig. 2). It is possible that the SI may secrete some known or unknown apos that are not secreted by the liver, and this proposition will need to be examined in future studies.

Our result that the two peptides (m/z 542 and m/z 524), which were detected as major peaks in SI-HDL obtained using our in situ perfusion model, were not detected in C-HDL obtained from the SI lymph duct in anesthetized mice (Fig. 2), suggests that rate of the production of HDL by the SI is slow as compared with that of filtration of preexisting liver-originated HDL from the abdominal aorta into the SI lymph duct, and thus liver-originated HDL is

predominant in the SI lymph duct in anesthetized mice. This finding explains the result of Brunham et al. (16) that lymph from mice that specifically lack ABCA1 in the liver had no detectable HDL-C.

Our finding, obtained with peptide mapping of HDL using LC/MS, that C-HDL was very similar to L-HDL but different from SI-HDL (Fig. 2) further confirms our finding, obtained by perfusion of ABCA1 KO mice with serum from WT mice, that plasma HDL can filtrate from the abdominal aorta into the SI lymph duct (Fig. 1C). Therefore, our novel findings indicate that our in situ perfusion model can selectively evaluate HDL produced from the SI without possible interference from plasma HDL or HDL derived from the liver.

Using the novel in situ perfusion model, we characterized SI-HDL in comparison with plasma HDL and L-HDL. We found that SI-HDL had a much higher protein content and a lower lipid content than plasma HDL and that CE and PL were the major lipids (Table 1, Fig. 4A). Consistent with these findings, by examining SI-HDL using EM, we found that most SI-HDL was spherical and HDL was smaller than plasma HDL (Fig. 5). Our finding that SI-HDL is small and dense compared with plasma HDL suggests that SI-HDL may have higher antiatherogenic activity than plasma HDL (52).

When mice were fed ad libitum, SI-HDL separated from lymph perfusates by ultracentrifugation contained more TG and less CE than that from liver perfusates (Table 1), suggesting that the composition of core lipids of intestinal HDL is different from that of hepatic HDL. It is possible that HDL becomes TG rich due to fusion between nascent HDL and TG-rich lipoprotein (TRL). We have previously shown that HDL reconstituted from apo AI and PLs remodels plasma apo-B-containing lipoprotein from a patient with Tangier disease, which was TG rich (53), and from a patient with hypercholesterolemia (35). TG in HDL is known to be hydrolyzed by hepatic TG lipase. A lack of hepatic TG lipase in SI lymph perfusates may also lead to TG-rich SI-HDL.

Our analyses of apos in ultracentrifugation density fractions of lipoproteins in SI lymph perfusates showed that apo AIV and apo AI were distributed in both the HDL and non-HDL fractions (Fig. 3B). We compared the compositions of apos of intestinal and hepatic HDL in HDL density fractions separated from SI lymph perfusates and liver perfusates from WT mice using ultracentrifugation (Fig. 4B). We found that L-HDL contained a very limited amount of apo AIV but a considerable amount of apo E, whereas an opposite trend was seen with SI-HDL (Fig. 4B).

Ohta et al. (54) showed that apo AIV exists as a complex with apo AI. They separated apo-AIV-containing HDL using an anti-apo AIV immunoabsorbance column from a human lymph TRL fraction, lymph lipoprotein-deficient fraction (LDF), plasma HDL, and plasma LDF and analyzed apos after separation by SDS-PAGE. Also, Böttcher et al. (55), who separated plasma HDL into charge-based subfractions using preparative isotachophoresis, showed that slow-migrating HDL contained both apo AIV and apo AI, whereas fast-migrating HDL contained only apo AI. However, Duka et al. (56) showed that apo-AIV-containing HDL is formed in the absence of apo AI by using apo $AI^{-/-}$ mice that had been transfected with the apo AIV gene. Therefore, apo AIV coexists with apo AI but can form HDL independent of apo AI if apo AI is absent. It would be interesting to know whether apo-AIV-containing HDL is formed in patients with a genetic apo AI deficiency.

Apo AIV, which is mainly expressed in the SI, is a 46 kDa plasma protein associated with CM and HDL (54, 57) and reportedly can inhibit lipid oxidation and enhance cholesterol efflux. In addition, the overexpression of apo AIV was found to reduce atherosclerosis in mice models (58–60). Therefore, it would be of considerable interest to determine the function and relevance of SI-HDL, particularly with respect to atherosclerosis.

Because the examination of SI-HDL by EM showed spherical particles (Fig. 5), we examined the involvement of ABCA1 and LCAT in the formation of SI-HDL by using inhibitors of ABCA1 and LCAT (Fig. 6). We found that in SI lymph perfusates from WT mice markedly increased levels of free apo AI were detected in the presence of an ABCA1 inhibitor in the perfusion buffer, and pre-β-HDL appeared in the presence of an LCAT inhibitor in the perfusion buffer (Fig. 6). This finding indicates that both ABCA1 and LCAT may be involved in the formation of SI-HDL (2).

Complete inhibition of ABCA1 or LCAT was not achieved in our experiments, and this may have been due to technical reasons; that is, the selection and dosage of inhibitors was limited because of the sensitivity of the SI to the organic solvents (methanol and ethanol) used for solving the inhibitors. However, because we have shown that SI-HDL is rich in apo AIV, our finding is consistent with that of Duka et al. (56), who showed that ABCA1 and LCAT participate in the biogenesis of apo-AIV-containing particles by using $ABCA1^{-/-}$ and $LCAT^{-/-}$ mice that had been transfected with the apo AIV gene.

Using this novel in situ perfusion model, we also found that fasting drastically reduced, and high-fat feeding drastically increased, HDL-apo AI and HDL-C levels in SI lymph perfusates from WT mice (Fig. 7A, B). Our findings indicate that the production of SI-HDL can be dynamically regulated by nutritional factors. It would be interesting to determine whether the ratio of apo AI in HDL to lipid-poor apo AI is similar under different dietary conditions. Our in situ perfusion model should be useful for further investigating the regulation of the production of SI-HDL by various diet components such as saturated and unsaturated fatty acids.

We found that the production of SI-HDL was markedly reduced in the major experimental murine model for atherosclerosis, apo E KO mice (Fig. 7C). Reduced HDL-apo AI and HDL-C in SI lymph perfusates from apo E KO mice may be caused by a redistribution of apos from HDL to non-HDL due to substantial hyperlipidemia and abnormal lipoprotein metabolism. Our results showed that apo AI in SI lymph perfusates was distributed in HDL in WT mice but was distributed in non-HDL in apo E KO mice (Fig. 7C). Duka et al. (56) showed that apo AIV was contained

in HDL in apo $AI^{-/-}$ mice but was redistributed to non-HDL in apo $AI^{-/-}$ × apo $E^{-/-}$ mice.

Using our in situ perfusion model, we obtained novel information regarding the production of HDL by the SI, the characteristics of SI-HDL, and the regulation of HDL. However, this model is limited because the effects of anesthesia on gut motility and intestinal lipid trafficking are not clear.

The inhibition of cholesteryl ester transfer protein (CETP) may be a strategy for raising HDL. However, it has been demonstrated that such a strategy needs to be reconsidered because some clinical trials with CETP inhibitors have failed and been terminated (61–63). We reported in the 1990s that genetic human CETP deficiency was atherogenic rather than beneficial (64–66). Based on both these previous and current studies, an increase in the production of SI-HDL may be a therapeutic target for raising HDL.

In summary, we have shown that our in situ perfusion model using surgically isolated mouse SI achieves the selective evaluation of HDL produced from the intestine. Using this model, we showed that the production of HDL from the SI in mice requires ABCA1, and that SI-HDL is different from HDL produced by the liver and is regulated by nutritional and genetic factors. Because the intestine is a promising target for raising HDL, our in situ perfusion model represents a useful tool for developing novel strategies for the prevention and treatment of atherosclerosis. In addition, the SI performs various important functions in not only lipid homeostasis (67) but also immune defense as well as the production of hormones and cytokines. Therefore, our novel in situ perfusion system, which can be used in other spontaneous and genetically engineered mouse models, may also be a useful research tool for investigating physiological and pathological conditions in the SI and adjacent organs.

The authors thank Drs. Seiichiro Tarui and Masao Kawasaki for their helpful comments and discussion, Dr. Kazumitsu Ueda for providing antibody against ABCA1, and Mr. Jan K. Visscher for editing and proofreading the manuscript.

REFERENCES

1. Rader, D. J. 2006. Molecular regulation of HDL metabolism and function: implications for novel therapies. *J. Clin. Invest.* **116:** 3090–3100.
2. Nicholls, S. J., K. A. Rye, and P. J. Barter. 2005. High-density lipoproteins as therapeutic targets. *Curr. Opin. Lipidol.* **16:** 345–349.
3. Miller, N. E. 1990. Raising high density lipoprotein cholesterol. The biochemical pharmacology of reverse cholesterol transport. *Biochem. Pharmacol.* **40:** 403–410.
4. Miller, G. J., and N. E. Miller. 1975. Plasma-high-density-lipoprotein concentration and development of ischaemic heart-disease. *Lancet.* **1:** 16–19.
5. Castelli, W. P., J. T. Doyle, T. Gordon, C. G. Hames, M. C. Hjortland, S. B. Hulley, A. Kagan, and W. J. Zukel. 1977. HDL cholesterol and other lipids in coronary heart disease. The cooperative lipoprotein phenotyping study. *Circulation.* **55:** 767–772.
6. Brooks-Wilson, A., M. Marcil, S. M. Clee, L. H. Zhang, K. Roomp, M. van Dam, L. Yu, C. Brewer, J. A. Collins, H. O. Molhuizen, et al. 1999. Mutations in ABC1 in Tangier disease and familial high-density lipoprotein deficiency. *Nat. Genet.* **22:** 336–345.
7. Bodzioch, M., E. Orso, J. Klucken, T. Langmann, A. Bottcher, W. Diederich, W. Drobnik, S. Barlage, C. Buchler, M. Porsch-Ozcurumez, et al. 1999. The gene encoding ATP-binding cassette transporter 1 is mutated in Tangier disease. *Nat. Genet.* **22:** 347–351.
8. Rust, S., M. Rosier, H. Funke, J. Real, Z. Amoura, J. C. Piette, J. F. Deleuze, H. B. Brewer, N. Duverger, P. Denefle, et al. 1999. Tangier disease is caused by mutations in the gene encoding ATP-binding cassette transporter 1. *Nat. Genet.* **22:** 352–355.
9. Murthy, S., E. Born, S. N. Mathur, and F. J. Field. 2002. LXR/RXR activation enhances basolateral efflux of cholesterol in CaCo-2 cells. *J. Lipid Res.* **43:** 1054–1064.
10. Ohama, T., K. Hirano, Z. Zhang, R. Aoki, K. Tsujii, Y. Nakagawa-Toyama, K. Tsukamoto, C. Ikegami, A. Matsuyama, M. Ishigami, et al. 2002. Dominant expression of ATP-binding cassette transporter-1 on basolateral surface of Caco-2 cells stimulated by LXR/RXR ligands. *Biochem. Biophys. Res. Commun.* **296:** 625–630.
11. Iqbal, J., K. Anwar, and M. M. Hussain. 2003. Multiple, independently regulated pathways of cholesterol transport across the intestinal epithelial cells. *J. Biol. Chem.* **278:** 31610–31620.
12. Johansson, C., S. Rossner, and G. Walldius. 1978. H.D.L. secretion from human intestinal tract. *Lancet.* **1:** 324–325.
13. Green, P. H., R. M. Glickman, C. D. Saudek, C. B. Blum, and A. R. Tall. 1979. Human intestinal lipoproteins. Studies in chyluric subjects. *J. Clin. Invest.* **64:** 233–242.
14. Green, P. H., A. R. Tall, and R. M. Glickman. 1978. Rat intestine secretes discoid high density lipoprotein. *J. Clin. Invest.* **61:** 528–534.
15. Timmins, J. M., J. Y. Lee, E. Boudyguina, K. D. Kluckman, L. R. Brunham, A. Mulya, A. K. Gebre, J. M. Coutinho, P. L. Colvin, T. L. Smith, et al. 2005. Targeted inactivation of hepatic Abca1 causes profound hypoalphalipoproteinemia and kidney hypercatabolism of apoA-I. *J. Clin. Invest.* **115:** 1333–1342.
16. Brunham, L. R., J. K. Kruit, J. Iqbal, C. Fievet, J. M. Timmins, T. D. Pape, B. A. Coburn, N. Bissada, B. Staels, A. K. Groen, et al. 2006. Intestinal ABCA1 directly contributes to HDL biogenesis in vivo. *J. Clin. Invest.* **116:** 1052–1062.
17. Joyce, C. W., E. M. Wagner, F. Basso, M. J. Amar, L. A. Freeman, R. D. Shamburek, C. L. Knapper, J. Syed, J. Wu, B. L. Vaisman, et al. 2006. ABCA1 overexpression in the liver of LDLr-KO mice leads to accumulation of pro-atherogenic lipoproteins and enhanced atherosclerosis. *J. Biol. Chem.* **281:** 33053–33065.
18. Lo Sasso, G., S. Murzilli, L. Salvatore, I. D'Errico, M. Petruzzelli, P. Conca, Z. Y. Jiang, L. Calabresi, P. Parini, and A. Moschetta. 2010. Intestinal specific LXR activation stimulates reverse cholesterol transport and protects from atherosclerosis. *Cell Metab.* **12:** 187–193.
19. Forester, G. P., A. R. Tall, C. L. Bisgaier, and R. M. Glickman. 1983. Rat intestine secretes spherical high density lipoproteins. *J. Biol. Chem.* **258:** 5938–5943.
20. Bearnot, H. R., R. M. Glickman, L. Weinberg, P. H. Green, and A. R. Tall. 1982. Effect of biliary diversion on rat mesenteric lymph apolipoprotein-I and high density lipoprotein. *J. Clin. Invest.* **69:** 210–217.
21. Sipahi, A. M., H. C. Oliveira, K. S. Vasconcelos, L. N. Castilho, A. Bettarello, and E. C. Quintao. 1989. Contribution of plasma protein and lipoproteins to intestinal lymph: comparison of long-chain with medium-chain triglyceride duodenal infusion. *Lymphology.* **22:** 13–19.
22. Vasconcelos, K. S., A. M. Sipahi, H. C. Oliveira, L. N. Castilho, N. De Luccia, and E. C. Quintao. 1989. Origin of intestinal lymph cholesterol in rats: contribution from luminal absorption, mucosal synthesis and filtration from plasma. *Lymphology.* **22:** 4–12.
23. Nutescu, E. A., N. L. Shapiro, and A. Chevalier. 2008. New anticoagulant agents: direct thrombin inhibitors. *Cardiol. Clin.* **26:** 169–187.
24. Kavin, H., N. W. Levin, and M. M. Stanley. 1967. Isolated perfused rat small bowel–technic, studies of viability, glucose absorption. *J. Appl. Physiol.* **22:** 604–611.
25. Windmueller, H. G., and A. E. Spaeth. 1972. Fat transport and lymph and plasma lipoprotein biosynthesis by isolated intestine. *J. Lipid Res.* **13:** 92–105.
26. Wang, N., D. L. Silver, C. Thiele, and A. R. Tall. 2001. ATP-binding cassette transporter A1 (ABCA1) functions as a cholesterol efflux regulatory protein. *J. Biol. Chem.* **276:** 23742–23747.
27. Dory, L., C. H. Sloop, L. M. Boquet, R. L. Hamilton, and P. S. Roheim. 1983. Lecithin:cholesterol acyltransferase-mediated modification of discoidal peripheral lymph high density lipoproteins: possible mechanism of formation of cholesterol-induced high density lipoproteins (HDLc) in cholesterol-fed dogs. *Proc. Natl. Acad. Sci. USA.* **80:** 3489–3493.
28. Sugano, T., K. Suda, M. Shimada, and N. Oshino. 1978. Biochemical and ultrastructural evaluation of isolated rat liver systems perfused with a hemoglobin-free medium. *J. Biochem.* **83:** 995–1007.

29. Rappsilber, J., M. Mann, and Y. Ishihama. 2007. Protocol for micro-purification, enrichment, pre-fractionation and storage of peptides for proteomics using StageTips. *Nat. Protoc.* **2:** 1896–1906.
30. Sano, S., S. Tagami, Y. Hashimoto, K. Yoshizawa-Kumagaye, M. Tsunemi, M. Okochi, and T. Tomonaga. 2014. Absolute quantitation of low abundance plasma APL1beta peptides at sub-fmol/mL level by SRM/MRM without immunoaffinity enrichment. *J. Proteome Res.* **13:** 1012–1020.
31. Usui, S., Y. Hara, S. Hosaki, and M. Okazaki. 2002. A new on-line dual enzymatic method for simultaneous quantification of cholesterol and triglycerides in lipoproteins by HPLC. *J. Lipid Res.* **43:** 805–814.
32. Okazaki, M., S. Usui, M. Ishigami, N. Sakai, T. Nakamura, Y. Matsuzawa, and S. Yamashita. 2005. Identification of unique lipoprotein subclasses for visceral obesity by component analysis of cholesterol profile in high-performance liquid chromatography. *Arterioscler. Thromb. Vasc. Biol.* **25:** 578–584.
33. Toshima, G., Y. Iwama, F. Kimura, Y. Matsumoto, M. Miura, J. Takahashi, H. Yasuda, N. Arai, H. Mizutani, K. Hata, et al. 2013. LipoSEARCH®; analytical GP-HPLC method for lipoprotein profiling and its applications. *J Biol Macromol.* **13:** 21–32.
34. Furusyo, N., M. Ai, M. Okazaki, H. Ikezaki, T. Ihara, T. Hayashi, S. Hiramine, K. Ura, T. Kohzuma, E. J. Schaefer, et al. 2013. Serum cholesterol and triglyceride reference ranges of twenty lipoprotein subclasses for healthy Japanese men and women. *Atherosclerosis.* **231:** 238–245.
35. Zhang, B., Y. Uehara, S. Hida, S. Miura, D. L. Rainwater, M. Segawa, K. Kumagai, K. A. Rye, and K. Saku. 2007. Effects of reconstituted HDL on charge-based LDL subfractions as characterized by capillary isotachophoresis. *J. Lipid Res.* **48:** 1175–1189.
36. Zhang, B., E. Kawachi, A. Matsunaga, S. Imaizumi, K. Noda, Y. Uehara, S. Miura, K. Yoshinaga, M. Kuroki, and K. Saku. 2012. Reactivity of direct assays for low-density lipoprotein (LDL) cholesterol toward charge-modified LDL in hypercholesterolemia. *Circ. J.* **76:** 2241–2248.
37. Zhang, B., A. Matsunaga, D. L. Rainwater, S. Miura, K. Noda, H. Nishikawa, Y. Uehara, K. Shirai, M. Ogawa, and K. Saku. 2009. Effects of rosuvastatin on electronegative LDL as characterized by capillary isotachophoresis: the ROSARY Study. *J. Lipid Res.* **50:** 1832–1841.
38. Zhang, B., A. Böttcher, S. Imaizumi, K. Noda, G. Schmitz, and K. Saku. 2007. Relation between charge-based apolipoprotein B-containing lipoprotein subfractions and remnant-like particle cholesterol levels. *Atherosclerosis.* **191:** 153–161.
39. Saku, K., B. Zhang, and K. Noda, and Patrol Trial Investigators. 2011. Randomized head-to-head comparison of pitavastatin, atorvastatin, and rosuvastatin for safety and efficacy (quantity and quality of LDL): the PATROL trial. *Circ. J.* **75:** 1493–1505.
40. Mills, G. L., P. A. Lane, and P. K. Weech. 1984. A guidebook to lipoprotein technique. *In* Laboratory Techniques in Biochemistry and Molecular Biology. R. H. Burdon and P. H. van Knippenberg, editors. Elsevier, New York, NY. 18–78.
41. Miida, T., K. Inano, T. Yamaguchi, T. Tsuda, and M. Okada. 1997. LpA-I levels do not reflect pre beta1-HDL levels in human plasma. *Atherosclerosis.* **133:** 221–226.
42. Miida, T., T. Yamada, U. Seino, M. Ito, Y. Fueki, A. Takahashi, K. Kosuge, S. Soda, O. Hanyu, K. Obayashi, et al. 2006. Serum amyloid A (SAA)-induced remodeling of CSF-HDL. *Biochim. Biophys. Acta.* **1761:** 424–433.
43. SAS Institute Inc. 2009. SAS Online Doc 9.2. SAS Institute Inc., Cary, NC.
44. Brunham, L. R., J. K. Kruit, T. D. Pape, J. S. Parks, F. Kuipers, and M. R. Hayden. 2006. Tissue-specific induction of intestinal ABCA1 expression with a liver X receptor agonist raises plasma HDL cholesterol levels. *Circ. Res.* **99:** 672–674.
45. McNeish, J., R. J. Aiello, D. Guyot, T. Turi, C. Gabel, C. Aldinger, K. L. Hoppe, M. L. Roach, L. J. Royer, J. de Wet, et al. 2000. High density lipoprotein deficiency and foam cell accumulation in mice with targeted disruption of ATP-binding cassette transporter-1. *Proc. Natl. Acad. Sci. USA.* **97:** 4245–4250.
46. Hirano, K., S. G. Young, R. V. Farese, Jr., J. Ng, E. Sande, C. Warburton, L. M. Powell-Braxton, and N. O. Davidson. 1996. Targeted disruption of the mouse apobec-1 gene abolishes apolipoprotein B mRNA editing and eliminates apolipoprotein B48. *J. Biol. Chem.* **271:** 9887–9890.
47. Shen, B. W., A. M. Scanu, and F. J. Kezdy. 1977. Structure of human serum lipoproteins inferred from compositional analysis. *Proc. Natl. Acad. Sci. USA.* **74:** 837–841.
48. Temel, R. E., and J. M. Brown. 2012. Biliary and nonbiliary contributions to reverse cholesterol transport. *Curr. Opin. Lipidol.* **23:** 85–90.
49. Bonamassa, B., and A. Moschetta. 2013. Atherosclerosis: lessons from LXR and the intestine. *Trends Endocrinol. Metab.* **24:** 120–128.
50. Granger, D. N., J. D. Valleau, R. E. Parker, R. S. Lane, and A. E. Taylor. 1978. Effects of adenosine on intestinal hemodynamics, oxygen delivery, and capillary fluid exchange. *Am. J. Physiol.* **235:** H707–H719.
51. Masuda, D., K. Hirano, H. Oku, J. C. Sandoval, R. Kawase, M. Yuasa-Kawase, Y. Yamashita, M. Takada, K. Tsubakio-Yamamoto, Y. Tochino, et al. 2009. Chylomicron remnants are increased in the postprandial state in CD36 deficiency. *J. Lipid Res.* **50:** 999–1011.
52. Kontush, A., P. Therond, A. Zerrad, M. Couturier, A. Negre-Salvayre, J. A. de Souza, S. Chantepie, and M. J. Chapman. 2007. Preferential sphingosine-1-phosphate enrichment and sphingomyelin depletion are key features of small dense HDL3 particles: relevance to antiapoptotic and antioxidative activities. *Arterioscler. Thromb. Vasc. Biol.* **27:** 1843–1849.
53. Uehara, Y., Y. Tsuboi, B. Zhang, S. Miura, Y. Baba, M. A. Higuchi, T. Yamada, K. A. Rye, and K. Saku. 2008. POPC/apoA-I discs as a potent lipoprotein modulator in Tangier disease. *Atherosclerosis.* **197:** 283–289.
54. Ohta, T., N. H. Fidge, and P. J. Nestel. 1984. Characterization of apolipoprotein A-IV complexes and A-IV isoforms in human lymph and plasma lipoproteins. *J. Biol. Chem.* **259:** 14888–14893.
55. Böttcher, A., J. Schlosser, F. Kronenberg, H. Dieplinger, G. Knipping, K. J. Lackner, and G. Schmitz. 2000. Preparative free-solution isotachophoresis for separation of human plasma lipoproteins: apolipoprotein and lipid composition of HDL subfractions. *J. Lipid Res.* **41:** 905–915.
56. Duka, A., P. Fotakis, D. Georgiadou, A. Kateifides, K. Tzavlaki, L. von Eckardstein, E. Stratikos, D. Kardassis, and V. I. Zannis. 2013. ApoA-IV promotes the biogenesis of apoA-IV-containing HDL particles with the participation of ABCA1 and LCAT. *J. Lipid Res.* **54:** 107–115.
57. Bisgaier, C. L., O. P. Sachdev, L. Megna, and R. M. Glickman. 1985. Distribution of apolipoprotein A-IV in human plasma. *J. Lipid Res.* **26:** 11–25.
58. Duverger, N., N. Ghalim, G. Ailhaud, A. Steinmetz, J. C. Fruchart, and G. Castro. 1993. Characterization of apoA-IV-containing lipoprotein particles isolated from human plasma and interstitial fluid. *Arterioscler. Thromb.* **13:** 126–132.
59. Qin, X., D. K. Swertfeger, S. Zheng, D. Y. Hui, and P. Tso. 1998. Apolipoprotein AIV: a potent endogenous inhibitor of lipid oxidation. *Am. J. Physiol.* **274:** H1836–H1840.
60. Duverger, N., G. Tremp, J. M. Caillaud, F. Emmanuel, G. Castro, J. C. Fruchart, A. Steinmetz, and P. Denefle. 1996. Protection against atherogenesis in mice mediated by human apolipoprotein A-IV. *Science.* **273:** 966–968.
61. Nissen, S. E., J. C. Tardif, S. J. Nicholls, J. H. Revkin, C. L. Shear, W. T. Duggan, W. Ruzyllo, W. B. Bachinsky, G. P. Lasala, E. M. Tuzcu, et al. 2007. Effect of torcetrapib on the progression of coronary atherosclerosis. *N. Engl. J. Med.* **356:** 1304–1316. [Erratum. 2007. *N. Engl. J. Med.* 357: 835.]
62. Barter, P. J., M. Caulfield, M. Eriksson, S. M. Grundy, J. J. Kastelein, M. Komajda, J. Lopez-Sendon, L. Mosca, J. C. Tardif, D. D. Waters, et al. 2007. Effects of torcetrapib in patients at high risk for coronary events. *N. Engl. J. Med.* **357:** 2109–2122.
63. Schwartz, G. G., A. G. Olsson, M. Abt, C. M. Ballantyne, P. J. Barter, J. Brumm, B. R. Chaitman, I. M. Holme, D. Kallend, L. A. Leiter, et al. 2012. Effects of dalcetrapib in patients with a recent acute coronary syndrome. *N. Engl. J. Med.* **367:** 2089–2099.
64. Hirano, K., S. Yamashita, Y. Kuga, N. Sakai, S. Nozaki, S. Kihara, T. Arai, K. Yanagi, S. Takami, M. Menju, et al. 1995. Atherosclerotic disease in marked hyperalphalipoproteinemia. Combined reduction of cholesteryl ester transfer protein and hepatic triglyceride lipase. *Arterioscler. Thromb. Vasc. Biol.* **15:** 1849–1856.
65. Hirano, K., S. Yamashita, N. Nakajima, T. Arai, T. Maruyama, Y. Yoshida, M. Ishigami, N. Sakai, K. Kameda-Takemura, and Y. Matsuzawa. 1997. Genetic cholesteryl ester transfer protein deficiency is extremely frequent in the Omagari area of Japan. Marked hyperalphalipoproteinemia caused by CETP gene mutation is not associated with longevity. *Arterioscler. Thromb. Vasc. Biol.* **17:** 1053–1059.
66. Hirano, K., S. Yamashita, and Y. Matsuzawa. 2000. Pros and cons of inhibiting cholesteryl ester transfer protein. *Curr. Opin. Lipidol.* **11:** 589–596.
67. Abumrad, N. A., and N. O. Davidson. 2012. Role of the gut in lipid homeostasis. *Physiol. Rev.* **92:** 1061–1085.

Increased Concentrations of Apo A-I and Apo A-II Fragments in the Serum of Patients With Hepatocellular Carcinoma by Magnetic Beads–Assisted MALDI-TOF Mass Spectrometry

Yang Liu, MD, PhD,[1,5] Kazuyuki Sogawa, PhD,[2,3] Masahiko Sunaga, MD, PhD,[2] Hiroshi Umemura, MD, PhD,[2] Mamoru Satoh, PhD,[2,3] Takahiro Kazami, MD, PhD,[2] Masaharu Yoshikawa, MD, PhD,[1] Takeshi Tomonaga, MD, PhD,[3,4] Osamu Yokosuka, MD, PhD,[1] and Fumio Nomura, MD, PhD[2,3]

From the Departments of [1]Medicine and Clinical Oncology and [2]Molecular Diagnosis, Graduate School of Medicine, Chiba University, Chiba, Japan; [3]Clinical Proteomics Center, Chiba University Hospital, Chiba; [4]Laboratory of Proteome Research, National Institute of Biomedical Innovation, Osaka, Japan; and [5]Basic Medicine College, Beihua University, Jilin City, China.

Key Words: Hepatocellular carcinoma; MALDI-TOF MS; Apolipoprotein A-I; Apolipoprotein A-II

DOI: 10.1309/AJCPBLFBNAP6N2UN

ABSTRACT

Objectives: *Recent advances in sophisticated technologies in proteomics should provide promising ways to discover novel markers for hepatocellular carcinoma (HCC) in the early diagnosis.*

Methods: *Serum peptide and protein profiling was conducted by matrix-assisted laser desorption/ionization time-of-flight mass spectrometry (MALDI-TOF MS). Profiling was carried out in a training set of 16 patients with HCC and a testing set of 15 patients with cirrhosis without HCC. All the patients were hepatitis C virus positive. Candidate peaks were processed to partial purification, followed by protein identification by amino acid sequence analysis. Immunoprecipitation was conducted to confirm the protein identity.*

Results: *Partial purification and protein identification revealed that one peak that was up-regulated in HCC sera both in the training and the testing sets was a fragment of apolipoprotein A-I (apo A-I). Immunoprecipitation confirmed this result.*

Conclusions: *MALDI-TOF MS analysis revealed that apo A-I is a potential novel serum marker of HCC. Combination of these pretreatments and the current magnet bead–assisted MALDI-TOF MS will further enhance the efficiency of biomarker discovery for HCC.*

Hepatocellular carcinoma (HCC) is the most common form of primary hepatic malignancy.[1] Because the majority of HCCs develop in cirrhotic livers, patients with liver cirrhosis are recommended to have examinations on a regular basis for early detection of HCC.[2]

The current methods for early detection of HCC rely on several tools combining imaging techniques and serologic markers. Imaging techniques are expensive, and ultrasonography is highly dependent on the ability of operators.[3,4] Therefore, sensitive and specific serum markers capable of detecting HCC at an early stage are desirable.

Serum tumor markers for detecting HCC are classified into 4 groups: oncofetal and glycoprotein antigens, enzymes or isoenzymes, genes, and cytokines. α-Fetoprotein (AFP) and des-γ-caroboxy prothrombin (DCP), also called protein induced by vitamin-K absence or antagonist-II, are 2 representative tumor markers for HCC. Although AFP is most widely used, serum AFP levels may be normal in up to 40% of patients with HCC, particularly during the early stages.[5,6] Furthermore, the specificity of AFP is not satisfactory because serum levels can be elevated in hepatitis and cirrhosis as well.[7] Although DCP is a useful adjunct to AFP in detecting HCC, elevated DCP level was found in only 28% to 50% of HCCs less than 3 cm in size.[8,9] DCP is also known as a prognostic factor for HCC.[10]

More recently, some other tumor markers, such as glypican 3,[11] γ-glutamyltransferase II,[12] α-1-fucosidase,[13] vascular endothelial growth factor,[14] and transforming growth factor β-1[15] have been proposed as complementary markers for AFP. Furthermore, the circulating messenger RNA (mRNA) markers, such as AFP-mRNA[16] and human telomerase reverse transcriptase mRNA,[17] have been shown to be

diagnostic and prognostic indicators of HCC. None of these markers are satisfactory enough in terms of sensitivity and specificity to replace AFP and DCP.

A *proteome* is the complete set of proteins found in a given cell type in any particular state. *Proteomics* is the systematic study of proteomes focusing on the large-scale identification and characterization of proteins through the measurement of protein expression and modifications in studied samples. Proteomic approaches have been used in an attempt to identify new diagnostic markers and therapeutic targets in various clinical fields.[18,19]

An increasing number of recent reports provide evidence that the proteomic approach offers promising tools to discover and identify possible biomarkers for HCC.[20] In particular, surface-enhanced laser desorption/ionization time-of-flight mass spectrometry (SELDI-TOF MS) is a representative example of a proteomics technique for the high-throughput fingerprinting of serum proteins and peptides.[21,22] We used SELDI technology to generate comparative protein profiles of consecutive serum samples obtained during abstinence from alcoholic patients and found some potential biomarker for excessive alcohol consumption.[23,24] Using this technique, several protein peaks leading to differentiation of patients with HCC from patients with cirrhosis alone have been discovered.[25-28] Although SELDI-TOF MS can rapidly analyze many samples at a time, it has several drawbacks including high cost, difficulty in further identifying proteins, and limitation in separating small peptides.

More recently, a new high-throughput workflow with matrix-assisted laser desorption/ionization–time-of-flight/time-of-flight mass spectrometry (MALDI-TOF/TOF MS) was established for discovering and identifying serum peptides.[29] This method uses magnetic beads with different chemical chromatographic surfaces instead of ProteinChip arrays (Bio-Rad, Hercules, CA). Protein selectively bound to the magnetic beads are eluted and analyzed with MALDI-TOF MS. Compared with the SELDI-TOF MS ProteinChip system, the cost is low and one can proceed to further protein identification relatively easily. We have used this system (ClinProt, Bruker Daltonics, Bremen, Germany) and have so far found some helpful biomarkers for multiple sclerosis,[30] alcoholism,[31] and gastric cancer.[32] Here, we took advantage of the ClinProt system and searched for novel markers for HCC.

Materials and Methods

Patients and Blood Sample Preparation

A total of 103 patients seen at the Division of Gastroenterology, Chiba University Hospital, Chiba, Japan, from June 2003 to March 2004 (training group) and May 2006 to March 2007 (testing group) were included. The training group consisted of 16 patients with HCC and 15 with liver cirrhosis; the testing group consisted of 34 patients with HCC and 38 with liver cirrhosis for the second study step; 41 healthy individuals were included as control subjects. All the patients were hepatitis C virus (HCV) positive. In patients with cirrhosis, HCC was ruled out on the basis of the results of intensive imaging studies. Clinical data from these 103 patients are presented in ▮Table 1▮ and ▮Table 2▮. Serum samples were obtained from each patient before treatment, were collected under standardized conditions, and were subjected to the same sample preparation procedures that we described previously.[33] Serum samples were stored in aliquots at –80°C. Written informed consent was obtained from each patient before beginning the study.

Serum Pretreatment with WCX Magnetic Beads by ClinProt Robot

We used weak cation exchange (WCX) magnetic beads (Bruker Daltonics) and performed serum peptide fractionation according to the manufacturer's protocol. A 5-μL serum sample was mixed with a 10-μL binding solution to which 5 μL of WCX magnetic beads were added, and the solution

▮Table 1▮
Clinical Features of Patients in the Training Group

Patient Characteristics	LC	HCC
No. of patients	15	16
M/F	7/8	13/3
Mean age, y	63.5 ± 10.9	67.9 ± 8.8
Child-Pugh (A/B/C)	9/6/0	11/5/0
Stage (I/II/III/IV)[a]		
AFP, ng/mL	18.0 ± 15.5	123.3 ± 120.8
DCP, mau/mL	16.8 ± 4.2	2054.6 ± 5304.0

AFP, α-fetoprotein; au, arbitrary units; DCP, des-gamma-carboxy prothrombin; HCC, hepatocellular carcinoma, with diagnosis according to 2002 American Joint Committee on Cancer/International Union for Cancer Control (AJCC/IUCC) system; LC, liver cirrhosis.
[a] Stage indicates AJCC/TNM cancer staging based on 2001 criteria.

▮Table 2▮
Clinical Features of Patients in the Testing Group

Patient Characteristics	Normal	LC	HCC
No. of patients	41	38	34
M/F	25/16	16/22	22/12
Mean age, y	57.5 ± 7.5	62.8 ± 9.1	71.8 ± 22.6
Child-Pugh (A/B/C)		24/10/4	16/12/6
Stage (I/II/III/IV)[a]			5/24/4/1
AFP, ng/mL	1.7 ± 1.6	36.8 ± 82.1	250.0 ± 360.5
DCP, mau/mL	19.9 ± 5.0	38.2 ± 43.1	259.7 ± 758.1

AFP, α-fetoprotein; au, arbitrary units; DCP, des-gamma-carboxy prothrombin; HCC, hepatocellular carcinoma, with diagnosis according to 2002 American Joint Committee on Cancer/International Union for Cancer Control (AJCC/IUCC) system; LC, liver cirrhosis.
[a] Stage indicates AJCC/TNM cancer staging based on 2001 criteria.

DOI: 10.1309/AJCPBLFBNAP6N2UN

was mixed. Next, the tube was placed in a magnetic bead separator to allow separation of the unbound solution, and the supernatant was removed. The beads were then washed three times with 100 μL of wash buffer, and proteins and peptides were eluted from the magnetic beads with 10 μL each of an elution solution and a stabilization solution. The eluate was diluted 1:10 in matrix solution 2-cyano-4-hydroxycinnamic acid (Bruker Daltonics). Then 1 μL of the mixture was spotted onto an AnchorChip target (Bruker Daltonics) and left for several minutes at room temperature until it dried. These procedures from bead fractionation to spotting were performed automatically using the ClinProt robot (Bruker Daltonics) under strictly controlled humidity, as previously described.[34]

Mass Spectrometry

The AnchorChip target plate was placed in an autoflex II TOF/TOF mass spectrometer (Bruker Daltonics) controlled with Flexcontrol 2.4 software (Bruker Daltonics). The instrument is equipped with a 337-nm nitrogen laser, delayed-extraction electronics, and a 25-Hz digitizer. The instrument was externally calibrated by means of standard procedures. All acquisitions were generated by an automated acquisition method included in the instrument software and based on averaging 700 randomized shots. The acquisition laser power was set between 25% and 35%. Spectra were acquired in positive linear mode in the mass range of *m/z* between 600 and 10,000. Peak clusters were completed using a second-pass peak section (signal to noise ratio >5). The relative peak intensities, normalized to a total ion current of *m/z* between 600 and 10,000, were expressed as an arbitrary unit (au). All measurements were performed using ClinProtools 2.0 software (Bruker Daltonics).

Data Analysis

All spectra obtained from MALDI-TOF MS were analyzed with Bruker Daltonics FlexAnalysis 2.0 software in automatic mode and ClinProtools 2.0 software (the data interpretation software of the MS–based ClinProt solutions for biomarker analysis), the former to detect the peak intensities of interest and the latter to compare the peaks across the spectra obtained from all samples. Intra-assay coefficient of variance for the particular peak was calculated using 31 different samples.

The discriminatory power for each putative marker was further described via receiver operating characteristic (ROC) area under the curve analysis. The ROC curve was generated using IBM SPSS Statistics 19 software (SPSS, Chicago, IL).

Protein Purification and Identification

After pretreatment with WCX magnetic beads four times, the serum sample of one patient with HCC was eluted and an 80-μL eluate was obtained. High-pressure liquid chromatography separations were performed on an automated Shiseido Nanospace SI-2 System (Shiseido Fine Chemicals, Tokyo, Japan). Injection was performed by an auto-sampler with a completely filled 100-μL injection loop. The eluate (80 μL) was directly loaded onto the Intrada WP-RP column (Imtakt, Kyoto, Japan). The reversed-phase separations for each flow-through were performed under a set of conditions using a multisegment elution gradient, with eluent A (0.1% trifluoroacetic acid [TFA] in water, vol/vol) and eluent B (0.08% TFA in 90% acetonitrile, vol/vol). The gradient conditions consisted of three steps with increasing concentrations of the eluent B: 5%, 5 minutes; 5% to 95%, 23 minutes; 95%, 11 minutes; and 5%, 21 minutes for re-equilibration of the column at a flow rate of 0.40 mL/min for a total runtime of 60 minutes.

The chromatograms were monitored at 218 nm, and 40 fractions were collected at 0.5-minute intervals from 19.1 to 39.1 minutes. Each fraction was dried in a centrifugal vacuum concentrator and stored at –80°C for subsequent MS analysis. Fractions rich in the peptide of interest were collected and subjected to NH_2-terminal amino acid sequence analysis in a Procise 494 cLC protein sequencing system (Applied Biosystems, Carlsbad, CA).

Immunoprecipitation

Immunocapturing kit MB-IAC Prot G (Bruker Daltonics) was used according to the manufacturer's protocol. At first, 15 μL of protein G beads (PB) was diluted in 100 μL immobilization buffer (IB). The 115-μL diluted PB was incubated with individual 5-μg samples of anti–apolipoprotein A-I (apo A-I) antibody (Abcam, Tokyo, Japan) and 5-μg samples of anti–apolipoprotein A-II (apo A-II, Abcam) antibody at room temperature with rotation for 1 hour and then washed with 100 μL of IB on the magnetic separator. A 25-μL serum sample (diluted 5 times) was added and incubated with anti–apo A-II antibody bound to PB for 2 hours. The tube was placed in the magnetic separator and the supernatant was collected. The 20-μL supernatant was incubated with anti–apo A-I antibody bound to PB for 2 hours. The tube was placed in the magnetic separator, and the supernatant was collected and used for further pretreatment with WCX magnetic beads.

Other Procedures

Serum levels of AFP and DCP were measured using commercial enzyme immunoassay kits (Fujirebio, Tokyo, Japan), with cutoff values set at 100 ng/mL and 40 mau [arbitrary units]/mL.

The significance of differences in the aforementioned analyses was examined using IBM SPSS Statistics 19. The overall diagnostic accuracy of each tumor marker was evaluated with ROC analysis using R statistical software, version

DOI: 10.1309/AJCPBLFBNAP6N2UN

2.12.1 (http://www.r-project.org/) with the pROC add-on package. $P < .05$ was considered significant in all analyses.

Results

Serum Protein Profiling with MALDI-TOF MS and Data Analysis

To determine proteomic patterns and discover a new HCC tumor marker, serum samples were fractionated using magnetic beads coated with WCX chromatography resins, followed by profiling of the mass spectral patterns of serum samples from 16 patients with HCC and 15 with cirrhosis. Using ClinProt software to analyze the peaks across the spectra obtained from the samples, we found a total of 26 peaks that differed significantly between the two patient groups as summarized in **Table 3** and **Table 4**.

To validate the results obtained in the training set, we conducted the same procedures using the test set samples. The candidate peaks selected in both the training and testing sets are summarized (Table 4; discriminatory peaks detected both in the training set and the testing set). Of the 10 peaks detected by MALDI-TOF MS with peak intensities of 1,000 or above, we focused on two consecutive peaks (*m/z* of 8,567 and 8,894) in which the difference between HCC and cirrhosis was striking and consistent. Representative mass spectra are shown in **Figure 1**.

Table 3
Discriminatory Peaks and *P* Values in the Training Set

Peaks Increased in HCC		Peaks Decreased in HCC	
m/z	*P*	m/z	*P*
8567.16	<.0001	759.78	<.0001
9024.26	<.001	786.09	<.0001
1628.33	<.01	808.23	<.0001
1741.71	<.01	1350.82	<.0001
2660.62	<.01	1451.22	<.0001
4955.92	<.01	1207.72	<.01
8711.65	<.01	1780.07	<.01
1884.05	<.05	1897.78	<.01
3240.01	<.05	3949.11	<.01
4293.88	<.05	6613.03	<.01
5793.00	<.05	1466.87	<.05
8894.67	<.05	2022.97	<.05
9246.83	<.05	4087.09	<.05

HCC, hepatocellular carcinoma.

Table 4
Discriminatory Peaks Detected in Both the Training and Testing Sets

Peaks Increased in HCC		Peaks Decreased in HCC	
m/z	*P*	*m/z*	*P*
2660.62	<.0001	1451.22	<.01
1628.33	<.001		
8711.65	<.001		
1741.71	<.01		
3240.01	<.01		
8567.16	<.01		
8894.67	<.01		
4293.88	<.05		
4955.92	<.05		

HCC, hepatocellular carcinoma.

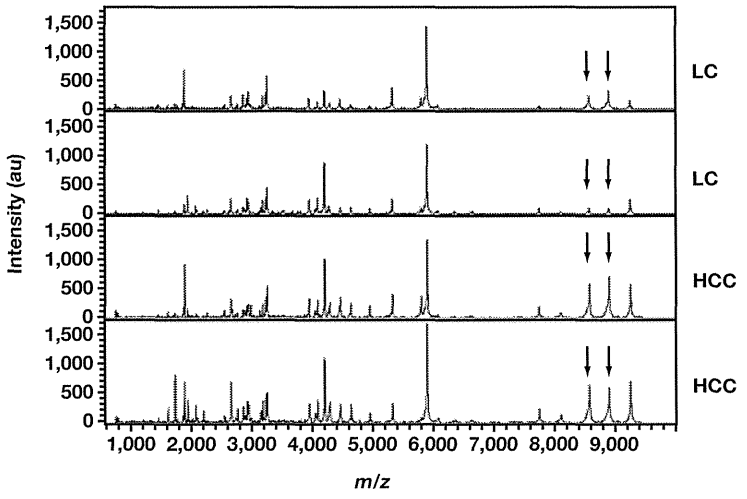

Figure 1 Representative matrix-assisted laser desorption/ionization (MALDI) spectra of serum samples obtained from two patients each with hepatocellular carcinoma (HCC) and liver cirrhosis (LC) in the training group. Mass spectra were generated with MALDI–time-of-flight mass spectrometry after prefractionation of serum samples using weak cation exchange magnetic beads with a ClinProt robot. The expression of the 8,567-Da and 8,894-Da peptides was greater in HCC than in LC (arrows). au, arbitrary units.

DOI: 10.1309/AJCPBLFBNAP6N2UN

Partial Purification and Identification of the Peaks of Interest

The peaks of interest were partially purified as outlined in the "Materials and Methods" section. Serum samples were first subjected to WCX magnetic beads, and the eluate was directly loaded onto the Intrada WP-RP column ▮**Figure 2A**▮. Under multisegment elution gradient conditions, the eluate was fractionated ▮**Figure 2B**▮. The fraction check during column chromatography was conducted with MALDI-TOF MS. Fractions rich in the peaks of interest were concentrated and subjected to NH_2-terminal amino acid sequence analysis in a Procise 494 cLC protein sequencing system. Amino acid sequencing of 8,567 Da revealed that it was a fragment of apo A-I ▮**Figure 2C**▮.

Immunoprecipitation

According to the literature, the 8,894-Da peak is likely to be a fragment of apo A-II.[35] Immunoprecipitation confirmed that the 8,894-Da peak was a fragment of Apo A-II. When HCC serum samples were incubated with sepharose beads coated with apo A-II mouse monoclonal antibody and centrifuged, in contrast to the serum samples without antibody treatment ▮**Figure 3A**▮, a fragment of apo A-II levels in the supernatant was minimal ▮**Figure 3B**▮.

The supernatant that had been immunoprecipitated with anti–apo A-II antibody was further immunoprecipitated with anti–apo A-I antibody. After these treatments, the peak intensity of the 8,567-Da peak was remarkably decreased, indicating that the 8,567-Da peak is indeed equivalent to a fragment of apo A-I ▮**Figure 3C**▮.

Comparison with AFP and DCP

Relative intensities of the 8,567-Da peak and 8,894-Da peak together with AFP and DCP data in 34 test set patients with HCC are presented in ▮**Table 5**▮.

▮**Figure 4**▮ shows the ROC curves for AFP, DCP, the 8,567-Da peak, and the 8,894-Da peak when the sensitivities were determined from the results of 34 patients with HCC,

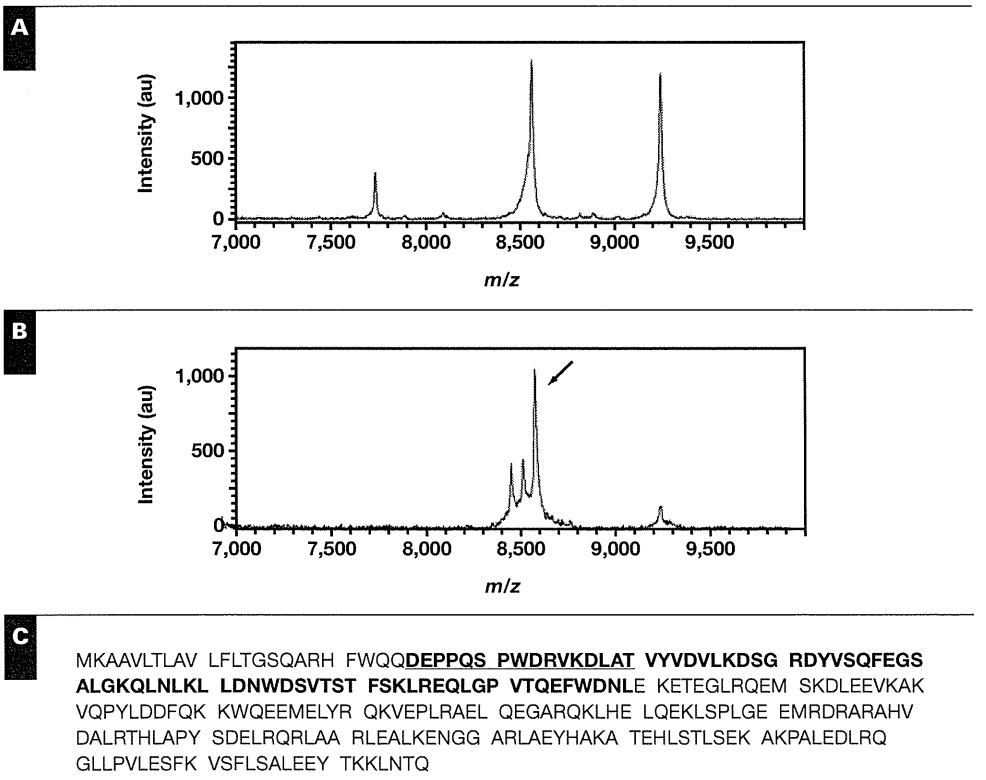

▮**Figure 2**▮ Partial purification of the 8,567-Da protein peaks. **A**, Matrix-assisted laser desorption/ionization–time-of-flight mass spectrometry spectrum of a serum sample with hepatocellular carcinoma after prefractionation with weak cation exchange magnetic beads. **B**, The eluate (total, 80 μL) was subjected to high-performance liquid chromatography and fractionated as described in the "Materials and Methods" section. The fraction (No. 19) rich in the specific protein (high peak) was collected (arrow). **C**, The No.19 fraction was concentrated and subjected to NH_2-terminal amino acid sequence analysis in a Procise 494 cLC protein sequencing system, which is matched by amino acid sequencing as shown in bold. au, arbitrary units.

DOI: 10.1309/AJCPBLFBNAP6N2UN

and specificities were based on 38 patients with cirrhosis. The areas under the curves for the 8,567-Da peak and the 8,894-Da peak were comparable with those for AFP and DCP. The ROC curves of AFP, DCP, the 8,567-Da peak, and the 8,894-Da peak were 0.682, 0.679, 0.660, and 0.648, respectively. The ROC curves of the AFP and DCP combination and the AFP, DCP, 8,567-Da peak, and 8,894-Da peak combination were 0.740 and 0.844, respectively ▮Figure 5▮.

The cutoff levels for the 8,567-Da and 8,894-Da peaks were set at the mean + two standard deviations of the data obtained in 38 patients with cirrhosis without HCC 924.8 au and 454.6 au, respectively. AFP levels were less than 100 ng/mL in 22 cases, and DCP levels were less than 40 IU/mL in 18 cases. In 16 cases, both AFP and DCP were not significantly elevated. It is noteworthy that among these 16 cases, both the 8,567-Da and 8,894-Da peaks were above the cutoff levels in three cases, and one of the two peaks was elevated in three cases. Thus, measurements of these peaks were complementary to AFP and DCP in six cases in which conventional tumor markers were not diagnostic.

When AFP and DCP were combined, their sensitivity and specificity were 52.9% and 76.3%, respectively. When AFP, DCP, the 8,567-Da peak, and the 8,894-Da peak were combined, the sensitivity and specificity were 67.6% and 76.3%, respectively.

Discussion

The sequencing of the human genome has opened the door for comprehensive transcriptome and proteome analysis. Transcriptome analyses have revealed unique patterns of gene expression that are clinically informative. mRNA abundances, however, are not necessarily predictive of corresponding protein abundances.[36] Because a detailed understanding of biological processes, both in healthy and pathologic states,

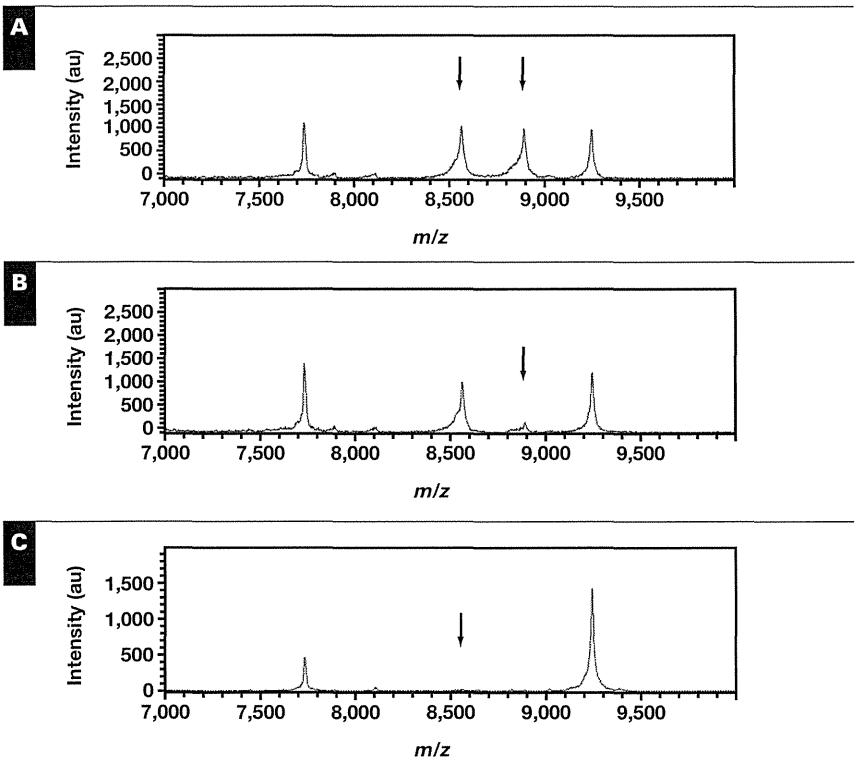

▮Figure 3▮ An immunoprecipitation assay was performed to confirm the 8,567-Da and 8,894-Da peaks. **A**, The baseline mass spectrum of serum samples with hepatocellular carcinoma (HCC) treated with protein-G sepharose beads and the cluster peaks of 8,567 Da and 8,894 Da showed high expression (arrows). **B**, Mass spectrum of supernatant after incubation of HCC serum samples with anti-apolipoprotein A-II antibody bound to protein-G sepharose beads. The 8,894-Da peak intensity was remarkably decreased (arrow). **C**, Mass spectrum of supernatant pretreated with anti-apolipoprotein A-II antibody after incubation of anti-apolipoprotein A-I antibody bound to protein-G sepharose beads. Compared with **A** and **B**, the 8,567-Da peak was disappearing, indicating that the 8,567-Da peak is indeed equivalent to apolipoprotein A-I (arrow). au, arbitrary units.

DOI: 10.1309/AJCPBLFBNAP6N2UN

requires the direct study of relevant proteins, proteomics bridges the gap between the information coded in the genome sequence and cellular behavior. Proteomics holds the promise of improving our understanding of HCC carcinogenesis and progression as well as discovering useful diagnostic and therapeutic markers.

Increasing numbers of studies have taken advantage of various proteomic technologies to discover and identify potential HCC markers.[20] Clinical tissue samples have been the most extensively studied samples in HCC proteomic studies. Most studies compared protein expression profiles of tumor tissues and adjacent nontumor tissues using two-dimensional electrophoresis and two-dimensional fluorescence difference gel electrophoresis.

Some studies used laser capture microdissection (LCM) to characterize isolated tumor cell populations from heterogenous tissue sections. By combining LCM and two-dimensional fluorescence difference gel electrophoresis, Liang et al[37] found that the protein profiles of well- and

Table 5
Relative Intensities of the 8,567-Da Peak and 8,894-Da Peak Together With AFP and DCP Data in Test Set Patients[a]

Case No.	Stage	AFP, ng/mL[b]	DCP, mau/mL[b]	8,567 Da, au	8,894 Da, au
1	I	1,200	75	353.7	603.5
2	I	52	26	1,018.1	797.6
3	I	28	20	147.7	206.6
4	I	16	407	68.5	239.5
5	I	42	35	481.7	244.8
6	II	255.9	247	19.7	24.9
7	II	3.8	25	687.9	111.3
8	II	162.8	76	653.9	357
9	II	26	32	620	89.2
10	II	7	13	989	529.8
11	II	42	26	576.9	639
12	II	6.5	16	1,043.4	731.1
13	II	45	20	1,152.1	233.7
14	II	28	880	573.7	188.2
15	II	457	551	573.1	243.6
16	II	63,670	520	762.6	401.6
17	II	141	104	1,230	350.5
18	II	182	52	1,654.5	509.8
19	II	200	138	615	342.4
20	II	37.6	23	738	257.9
21	II	93	14	28.7	51.6
22	II	7.9	4,401	161.7	162.8
23	II	649	14	23.7	14.2
24	II	6.4	227	1,607.3	875.2
25	II	3.4	144	530.5	254.3
26	II	11.6	11	246	107.6
27	II	19.6	26	150.5	181.9
28	II	10.7	10	439	309.5
29	II	1,313	12	561.3	733.2
30	IIIA	927	354	296.3	413.7
31	IIIA	206,300	252	416.5	97.3
32	IIIA	4.3	26	49.3	22.2
33	IIIB	21	12	1,918.5	155
34	IVB	28	41	1,551.9	265.9

AFP, α-fetoprotein; au, arbitrary units; DCP, des-γ-carboxy prothrombin.
[a] Data shown are for 34 patients with hepatocellular carcinoma in the test set. In the six cases shown in bold (cases 2, 10, 11, 12, 13, and 33), both AFP and DCP were not diagnostically elevated, whereas the 8,567-Da and/or 8,894-Da peaks were above the cutoff level.
[b] AFP and DCP were determined using commercial enzyme immunoassay kits (Fujirebio, Tokyo, Japan), and 100 ng/mL and 40 mau/mL, respectively, were considered the upper limit of normal.

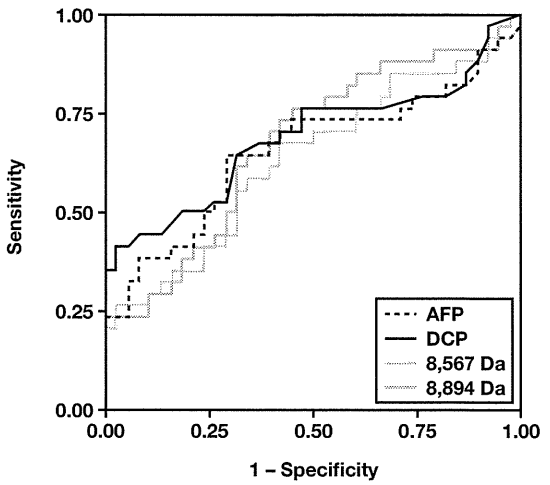

Figure 4 Receiver operating characteristic curve analysis for α-fetoprotein (AFP), des-γ-carboxy prothrombin (DCP), the 8,567-Da peak, and the 8,894-Da peak, with sensitivities were determined from the results of 34 patients with hepatocellular carcinoma and specificities based on 38 patients with liver cirrhosis.

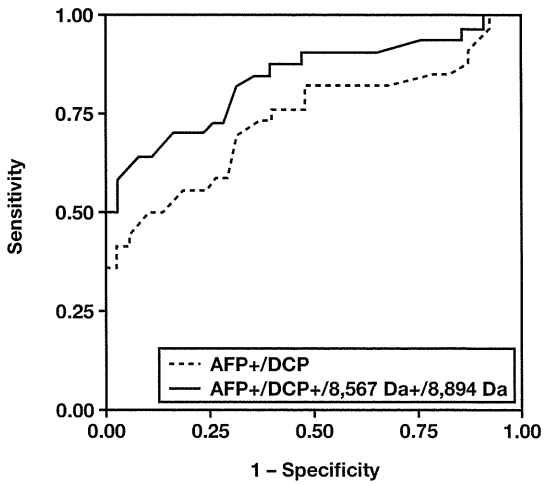

Figure 5 The receiver operating characteristic curves for combined α-fetoprotein (AFP) and des-γ-carboxy prothrombin (DCP) and combined AFP, DCP, 8,567-Da peak, and 8,894-Da peak, with sensitivities determined from the results of 34 patients with hepatocellular carcinoma and specificities based on 38 patients with liver cirrhosis.

DOI: 10.1309/AJCPBLFBNAP6N2UN

poorly differentiated HCC tissues are significantly different. Proteome analyses of tumor tissues should be a basis for HCC marker discovery, and a number of proteins have been identified as candidate markers for HCC.[38,39] We conducted proteome analyses to compare protein expressions of surgically resected HCC tissues and adjacent nontumor tissues using agarose two-dimensional fluorescence difference gel elecetrophoresis.[40] Expression levels of 83 proteins were found to differ between tumor and nontumor; immunoblot confirmed that the expression of clathrin heavy chain and Ku 86 significantly increased, whereas formiminotransferase cyclodeaminase, rhodanese, and vinculin decreased in tumor.[40] These histologic markers, however, have not been shown to be useful at serum levels as markers for HCC detection.

Plasma or serum is a target for extensive proteome analysis. SELDI-TOF MS has been successfully used to identify various cancers, such as prostate, ovarian, colon, breast, and pancreatic. SELDI-TOF MS has also been used to explore detective tumor markers in HCC. Poon et al[25] used IMAC3 Cu and WCX2 chips to identify tumor-specific proteomic signatures that can differentiate HCC from chronic liver diseases without HCC.

Paradis et al[26] found that the C-terminal fragment of vitronectin is a diagnostic marker for HCC. They also showed in an in vitro study that the vitronectin fragment was a cleavage product of intact vitronectin and metalloprotease that was overexpressed in HCC tissues.

More recently, Kanmura et al[27] analyzed serum samples obtained from seven patients with HCC before the diagnosis was made with ultrasonography. Cui et al[28] also conducted a SELDI-based search for HCC tumor markers. This technology, however, has some limitations; high cost, the fact that only one MS pass is made, and difficulty in further identifying proteins.

Instead of the chip-based method used in SELDI-TOF MS, the affinity bead–based approach analyzes serum samples with MALDI-TOF MS after fractionation using magnetic beads.[28] This technique has been used for identification and pattern recognition in various disease conditions, such as brain tumor[28] and oral cancer.[41] We also have used this technology and reported novel markers for multiple sclerosis,[30] alcoholism,[31] and gastric cancer.[32]

In this study, serum samples were fractionated using magnetic beads coated with WCX chromatography resins, followed by profiling of the mass spectral patterns of serum samples from 16 patients with HCC and 15 with cirrhosis as a training set. The candidate discriminatory peaks were validated in a test set. As a result, we found 10 peaks that differed significantly between the two patients groups as summarized in Table 4. The next step was to identify these peaks. Partial purification of the peaks of interest showed that the 8,567-Da peak was a fragment of apo A-I. The results of the immunoprecipitation experiment indicated that the 8,894-Da peak was a fragment of apo A-II.

Steel et al[42] suggested that apo A-I had a diagnostic role in patients with HCC. In their study, serum proteome analyses were conducted using two-dimensional electrophoresis in serum samples obtained from hepatitis B virus–positive individuals with varying levels of risk for the development of HCC and also from patients with HCC. The molecular weight of the apo A-I isoform presented in their report was different from the isoform presented herein. Also, serum levels of their apo A-I isoform were indeed lower in patients with HCC than those in patients with chronic hepatitis B.[42]

The 8,894-Da peak, most likely to be a fragment of apo A-II based on the result of the immunoprecipitation experiment, was reported to be overexpressed in serum samples from patients with prostate cancer.[35] It has been claimed that the peptide peak was elevated in patients with normal prostate-specific antigen levels, suggesting potential usefulness of the marker in detecting indolent disease.[35] Similar to our results, Malik et al[35] found the greatest discriminatory value in the study between normal and diseased, and some separation was found using the 8,900 *m/z* peak between benign prostatic hyperplasia. These studies suggest that a proteomic method can be used for identifying serum biomarkers for HCC and other liver diseases and also for distinguishing the HCC plus HCV-positive cirrhosis from HCV-positive cirrhosis.

Although the diagnostic abilities of these peptides as determined by ROC analysis were comparable with the two representative conventional markers, it is notable that both the 8,567-Da or 8,894-Da peaks were elevated in six of 16 cases in which both AFP and DCP were below their cutoff levels. These results suggest that the two peptides found in this study may be complementary to AFP and DCP in detecting HCC. Prospective studies with large numbers of cases will be necessary to further establish the diagnostic roles of the 8,567-Da and 8,894-Da peptides in the diagnosis of HCC. Also, it needs to be tested whether these peptides are altered in cancers other than those of the liver.

Address reprint requests to Dr Nomura: Dept of Molecular Diagnosis, Graduate School of Medicine, Division of Laboratory Medicine, Clinical Genetic and Proteomics, Chiba University Hospital, 1-8-1 Inohana, Chiba City, Chiba 260-8670, Japan; fnomura@faculty.chiba-u.jp.

Acknowledgments: The authors thank Fumie Iida and Manami Miura for their technical support.

References

1. Gomaa AI, Khan SA, Toledano MB, et al. Hepatocellular carcinoma: epidemiology, risk factors and pathogenesis. *World J Gastroenterol*. 2008;14:4300-4308.

2. Sangiovanni A, Ninno ED, Fasani P, et al. Increased survival of cirrhotic patients with a hepatocellular carcinoma detected during surveillance. *Gastroenterology*. 2004;126:1005-1014.
3. Sherman M. Hepatocellular carcinoma: epidemiology, risk factors, and screening. *Semin Liver Dis*. 2005;25:143-154.
4. Szklaruk J, Silverman PM, Charnsangavej C. Imaging in the diagnosis, staging, treatment, and surveillance of hepatocellular carcinoma. *AJR Am J Roentgenol*. 2003;180:441-454.
5. Nomura F, Ohnishi K, Tanabe Y. Clinical features and prognosis of hepatocellular carcinoma with reference to serum alpha-fetoprotein levels: analysis of 606 patients. *Cancer*. 1989;64:1700-1707.
6. Sherman M, Peltekian KM, Lee C. Screening for hepatocellular carcinoma in chronic carriers of hepatitis B virus: incidence and prevalence of hepatocellular carcinoma in a North American urban population. *Hepatology*. 1995;22:432-438.
7. Di Bisceglie AM, Hoofnagle JH. Elevations in serum alpha-fetoprotein levels in patients with chronic hepatitis B. *Cancer*. 1989;64:2117-2120.
8. Tsai SL, Huang GT, Yang PM, et al. Plasma des-γ-carboxyprothrombin in the early stage of hepatocellular carcinoma. *Hepatology*. 1990;11:481-488.
9. Nomura F, Ishijima M, Kuwa K, et al. Serum des-gamma-carboxy prothrombin levels determined by a new generation of sensitive immunoassays in patients with small-sized hepatocellular carcinoma. *Am J Gastroenterol*. 1999;94:650-654.
10. Hakamada K, Kimura N, Miura T, et al. Des-gamma-carboxy prothrombin as an important prognostic indicator in patients with small hepatocellular carcinoma. *World J Gastroenterol*. 2008;14:1370-1377.
11. Hippo Y, Watanabe K, Watanabe A, et al. Identification of soluble NH_2-terminal fragment of glypican-3 as a serological marker for early-stage hepatocellular carcinoma. *Cancer Res*. 2004;64:2418-2423.
12. Cui R, He J, Zhang F, et al. Diagnostic value of protein induced by vitamin K absence (PIVKAII) and hepatoma-specific band of serum gamma-glutamyl transferase (GGT) as hepatocellular carcinoma markers complementary to α-fetoprotein. *Br J Cancer*. 2003;88:1878-1882.
13. Ishizuka H, Nakayama T, Matsuoka S, et al. Prediction of the development of hepato-cellular-carcinoma in patients with liver cirrhosis by the serial determinations of serum alpha-L-fucosidase activity. *Intern Med*. 1999;38:927-931.
14. Jinno K, Tanimizu M, Hyodo I, et al. Circulating vascular endothelial growth factor (VEGF) is a possible tumor marker for metastasis in human hepatocellular carcinoma. *J Gastroenterol*. 1998;33:376-382.
15. Song BC, Chung YH, Kim JA, et al. Transforming growth factor-β1 as a useful serologic marker of small hepatocellular carcinoma. *Cancer*. 2002;94:175-180.
16. Ding X, Yang LY, Huang GW, et al. Role of AFP mRNA expression in peripheral blood as a predictor for postsurgical recurrence of hepatocellular carcinoma: a systematic review and meta-analysis. *World J Gastroenterol*. 2005;11:2656-2661.
17. Miura N, Maeda Y, Kanbe T, et al. Serum human telomerase reverse transcriptase messenger RNA as a novel tumor marker for hepatocellular carcinoma. *Clin Cancer Res*. 2005;11:3205-3209.
18. Smith L, Lind MJ, Welham KJ, et al; for the Cancer Biology Proteomics Group. Cancer proteomics and its application to discovery of therapy response markers in human cancer. *Cancer*. 2006;107:232-241.
19. Diamond DL, Proll SC, Jacobs JM, et al. HepatoProteomics: applying proteomic technologies to the study of liver function and disease. *Hepatology*. 2006;44:299-308.
20. Feng JT, Shang S, Beretta L. Proteomics for the early detection and treatment of hepatocellular carcinoma. *Oncogene*. 2006;25:3810-3817.
21. Reymond MA, Schlegel W. Proteomics in cancer. *Adv Clin Chem*. 2007;44:103-142.
22. Nomura F, Tomonaga T, Sogawa K, et al. Application of proteomic technologies to discover and identify biomarkers for excessive alcohol consumption: a review. *J Chromatogr B Analyt Technol Biomed Life Sci*. 2007;855:35-41.
23. Nomura F, Tomonaga T, Sogawa K, et al. Identification of novel and downregulated biomarkers for alcoholism by surface enhanced laser desorption/ionization-mass spectrometry. *Proteomics*. 2004;4:1187-1194.
24. Sogawa K, Itoga S, Tomonaga T, et al. Diagnostic values of surface-enhanced laser desorption/ionization technology for screening of habitual drinkers. *Alcohol Clin Exp Res*. 2007;31(suppl 1):S22-S26.
25. Poon TC, Yip TT, Chan AT, et al. Comprehensive proteomic profiling identifies serum proteomic signatures for detection of hepatocellular carcinoma and its subtypes. *Clin Chem*. 2003;49:752-760.
26. Paradis V, Degos F, Dargère D, et al. Identification of a new marker of hepatocellular carcinoma by serum protein profiling of patients with chronic liver diseases. *Hepatology*. 2005;41:40-47.
27. Kanmura S, Uto H, Kusumoto K, et al. Early diagnostic potential for hepatocellular carcinoma using the SELDI ProteinChip system. *Hepatology*. 2007;45:948-956.
28. Cui JF, Liu YK, Zhou HJ, et al. Screening serum hepatocellular carcinoma-associated proteins by SELDI-based protein spectrum analysis. *World J Gastroenterol*. 2008;14:1257-1262.
29. Villanueva J, Philip J, Entenberg D, et al. Serum peptide profiling by magnetic particle-assisted, automated sample processing and MALDI-TOF mass spectrometry. *Anal Chem*. 2004;76:1560-1570.
30. Sawai S, Umemura H, Mori M, et al. Serum levels of complement C4 fragments correlate with disease activity in multiple sclerosis: proteomic analysis. *J Neuroimmunol*. 2010;218:112-115.
31. Sogawa K, Satoh M, Kodera Y, et al. A search for novel markers of alcohol abuse using magnetic beads and MALDI-TOF/TOF mass spectrometry. *Proteomics Clin Appl*. 2009;3:821-828.
32. Umemura H, Togawa A, Sogawa K, et al. Identification of a high molecular weight kininogen fragment as a marker for early gastric cancer by serum proteome analysis. *J Gastroenterol*. 2011;46:577-585.
33. Umemura H, Nezu M, Kodera Y, et al. Effects of the time intervals between venipuncture and serum preparation for serum peptidome analysis by matrix-assisted laser desorption/ionization time-of-flight mass spectrometry. *Clin Chim Acta*. 2009;406:179-180.
34. Umemura H, Kodera Y, Nomura F. Effects of humidity on the dried-droplet sample preparation for MALDI-TOF MS peptide profiling. *Clin Chim Acta*. 2010;411:2109-2111.
35. Malik G, Ward MD, Gupta SK, et al. Serum levels of an isoform of apolipoprotein A-II as a potential marker for prostate cancer. *Clin Cancer Res*. 2005;11:1073-1085.

DOI: 10.1309/AJCPBLFBNAP6N2UN

36. Chen G, Gharib TG, Huang CC, et al. Discordant protein and mRNA expression in lung adenocarcinomas. *Mol Cell Proteomics*. 2002;1:304-313.
37. Liang CR, Leow CK, Neo JC, et al. Proteome analysis of human hepatocellular carcinoma tissues by two-dimensional difference gel electrophoresis and mass spectrometry. *Proteomics*. 2005;5:2258-2271.
38. Kim J, Kim SH, Lee SU, et al. Proteome analysis of human liver tumor tissue by two-dimensional gel electrophoresis and matrix assisted laser desorption/ionization-mass spectrometry for identification of disease-related proteins. *Electrophoresis*. 2002;23:4142-4156.
39. Lee IN, Chen CH, Sheu JC, et al. Identification of human hepatocellular carcinoma-related biomarkers by two-dimensional difference gel electrophoresis and mass spectrometry. *J Proteome Res*. 2005;4:2062-2069.
40. Seimiya M, Tomonaga T, Matsushita K, et al. Identification of novel immunohistochemical tumor markers for primary hepatocellular carcinoma: clathrin heavy chain and formiminotransferase cyclodeaminase. *Hepatology*. 2008;48:519-530.
41. Cheng AJ, Chen LC, Chien KY, et al. Oral cancer plasma tumor marker identified with bead-based affinity-fractionated proteomic technology. *Clin Chem*. 2005;51:2236-2244.
42. Steel LF, Shumpert D, Trotter M, et al. A strategy for the comparative analysis of serum proteomes for the discovery of biomarkers for hepatocellular carcinoma. *Proteomics*. 2003;3:601-609.

DOI: 10.1309/AJCPBLFBNAP6N2UN

RESEARCH ARTICLE

Serum Periplakin as a Potential Biomarker for Urothelial Carcinoma of the Urinary Bladder

Kazumasa Matsumoto[1]*, Masaomi Ikeda[1], Toshihide Matsumoto[2], Ryo Nagashio[3], Takanori Nishimori[5], Takeshi Tomonaga[7], Fumio Nomura[6], Yuichi Sato[3], Hidero Kitasato[4], Masatsugu Iwamura[1]

Abstract

The objectives of this study were to examine serum periplakin expression in patients with urothelial carcinoma of the urinary bladder and in normal controls, and to examine relationships with clinicopathological findings. Detection of serum periplakin was performed in 50 patients and 30 normal controls with anti-periplakin antibodies using the automatic dot blot system, and a micro-dot blot array with a 256 solid-pin system. Levels in patients with urothelial carcinoma of the urinary bladder were significantly lower than those in normal controls (0.31 and 5.68, respectively; p<0.0001). The area under the receiver-operator curve level for urothelial carcinoma of the urinary bladder was 0.845. The sensitivity and specificity, using a cut-off point of 4.045, were 83.7% and 73.3%, respectively. In addition, serum periplakin levels were significantly higher in patients with muscle-invasive cancer than in those with nonmuscle-invasive cancer (P = 0.03). In multivariate Cox proportional hazards regression analysis, none of the clinicopathological factors was associated with an increased risk for progression and cancer-specific survival. Examination of the serum periplakin level may play a role as a non-invasive diagnostic modality to aid urine cytology and cystoscopy.

Keywords: Periplakin - urothelial carcinoma - diagnosis

Asian Pac J Cancer Prev, **15 (22)**, 9927-9931

Introduction

Urothelial carcinoma of the urinary bladder (UCB) is the second most common malignancy in the genitourinary tract. Approximately 75% of UCB cases are diagnosed as nonmuscle-invasive bladder cancer (NMIBC) at the first diagnosis (Shelley et al., 2010). NMIBC has the tendency to recur and may progress to muscle-invasive bladder cancer (MIBC), which is a life-threatening neoplasm (Ikeda et al., 2014). Cystoscopy and urine cytology are typical modalities for the diagnosis and surveillance of UCB. Cystoscopy can identify the most papillary and solid lesions, but it is physically uncomfortable for patients. Use of urine cytology is limited because of its low sensitivity. For these reasons, some tumor markers have been investigated (eg, BTAstat, NMP22), but their sensitivity and specificity are limited and not superior to urine cytology (Toma et al., 2004). To overcome these limitations, preoperative molecular markers are expected to be used as a minimally invasive method for assisting in and predicting a precise diagnosis in patients with UCB (Ghafouri-Fard et al., 2014).

The plakin family mediates the tissue filaments that represent the cell cytoskeleton in cell-to-cell junctions mediated by cadherin, and it is able to withstand mechanical stimulation and provide integrity of tissues (Jefferson et al., 2004; Sonnenberg et al., 2007). Dysfunctional plakin proteins contribute to diverse diseases, and autoantibodies and mutations perturb their activities with profound consequences. Seven plakin proteins are found in mammalian cells. Envoplakin, desmoplakin, and periplakin are associated with desmosomes in various solid tissues. A proteomics technique including two-dimensional gel electrophoresis (2-DE) combined with immunoblot analysis has been shown to identify tumor-associated antigenic proteins for UCB (Minami et al., 2014). Periplakin is a candidate for being a tumor marker in patients with UCB. The 195-kDa membrane-associated protein periplakin is involved in cellular movement and attachment (Nagata et al., 2001).

We previously found that loss of periplakin expression was associated with biological aggressiveness of UCB using immunohistochemical staining (Matsumoto et al., 2014). In addition, the majority of UCB showed loss or

*[1]Departments of Urology and [2]Pathology, School of Medicine and Departments of [3]Molecular Diagnostics and [4]Microbiology, School of Allied Health Sciences, Kitasato University, Departments of [5]Frontier Surgery and [6]Molecular Diagnosis, Graduate School of Medicine, Chiba University, [7]National Institute of Biomedical Innovation, Laboratory of Proteome Research, Japan *For correspondence: kazumasa@cd5.so-net.ne.jp*

decreased expression patterns compared with normal or benign lesions on pathological slides. Next, we sought to determine whether the dynamics of serum periplakin would detect UCB and predict the prognosis in patients with UCB.

The primary objective of this study was to investigate the circulating periplakin levels needed for use as a potential detection marker for UCB. The secondary objective was to determine whether the levels of periplakin would be associated with clinicopathological features and prognosis in patients with UCB.

Materials and Methods

Patients

This retrospective study included 52 patients with UCB who were treated at Kitasato University Hospital between August 2004 and July 2009. Serum samples from two patients (a man and a woman) were used in other studies (Tsumura et al., 2014). There were 43 men (86%) and 7 women (14%) with a median age of 70 years (mean=68.5; range=39–82 years). Twenty-two of these patients were treated with radical cystectomy and bilateral pelvic lymphadenectomy, and the other 28 were treated with transurethral resection (TUR). Preoperative serum levels of periplakin were measured. Laboratory studies, chest X-ray, and pelvic computed tomography or magnetic resonance imaging were routinely investigated, and there was no evidence of clinical distant or lymph node metastasis in any of the patients. The 2002 Tumor–Node–Metastasis (TNM) classification was used for pathological staging, and the World Health Organization classification was used for pathological grading. Lymphovascular invasion (LVI) determined the presence of cancer cells within the endothelial space. Cancer cells that merely invaded a vascular lumen were considered negative.

The median follow-up time was 63.3 months (mean=60.9; range=6.4-125.9 months) for those patients who were still alive at the last follow-up session. A postoperative follow-up examination was scheduled every 3 to 4 months after TUR and cystectomy, respectively, during the first year. Semi-annual examinations were performed during the second year, with annual examinations thereafter. More frequent examinations were scheduled if clinically indicated. None of the patients had previous radiation or systemic chemotherapy before surgical treatment, and none had a history of pulmonary or skin diseases.

We also measured serum periplakin levels in 30 normal controls (healthy volunteers). Approval was granted by the ethics committee of Kitasato University School of Medicine and Hospital, and all patients signed written informed consent.

Measurement of serum periplakin

All serum samples were kept at -80°C until use. Serum periplakin levels were detected by using an automated micro-dot blot array with a 256 solid-pin system (Kakengeneqs Co., Ltd., Chiba, Japan). In brief, the removal of albumin and IgG from sera was performed using a ProteoExtract Albumin/IgG removal kit (Merck, Darmstadt, Germany) according to the manufacturer's instructions; 1 μl each of 20-times diluted albumin-depleted and IgG-depleted sera was spotted onto polyvinylidene difluoride membranes (Millipore Corp., Bedford, MA, USA). The membranes were then blocked with 20% N101 (NOF Corp., Tokyo, Japan)/ TBS for 1 h at room temperature. After being washed in TBS, the membranes were reacted with 100-times diluted primary polyclonal antibody against periplakin (Santa Cruz Biotech, Dallas, TX, USA) with 1% N101/TBS for 30 min at room temperature. After being washed with TBS containing 0.1% Tween-20, the membranes were incubated with 1000-times diluted horseradish peroxidase–conjugated anti-mouse IgG polyclonal antibody (Dako, Glostrup, Denmark) for 30 min at room temperature. Finally, signals were developed with Immobilon Western reagent (Millipore Corp.). The data were analyzed using DotBlotChip System software version 4.0 (Dynacom Co., Ltd., Chiba, Japan). Normalized signals are presented as the positive intensity minus background intensity around the spot.

Statistical analyses

For the purposes of our analysis, gender, age (younger than 65 versus 65 or older), pathological stage (Ta or T1 as NMIBC versus T2 or greater as MIBC), pathological grade (grades 1 and 2 versus grade 3), LVI (positive versus negative), and lymph node status (N0 versus N1 and N2) were evaluated as dichotomized variables. Mann-Whitney U test was used to evaluate the association of periplakin with gender, age, pathological stage and grade, lymph node status, and LVI. Mann-Whitney U test was also used to compare the serum periplakin levels between UCB patients and normal controls. The Kaplan Meier method was used to calculate survival functions, and differences were assessed with the log rank test. The area under the curve (AUC) and best cut-off point were calculated using the receiver-operating characteristic (ROC) analysis. Multivariate survival analyses were performed with the Cox proportional hazards regression model, controlling for serum periplakin, pathological stage and grade, presence of LVI, and lymph node metastases. Statistical significance was set as $p<0.05$. All analyses were performed with StatView (version 5.0; SAS Institute, Cary, NC, USA).

Results

Validation of preoperative serum periplakin

The median levels of serum periplakin in patients with UCB and in normal controls were 0.31 (mean=1.96; range=0–20.49) and 5.68 (mean=6.11; range=0–17.59), respectively (Figure 1). There were significantly decreased serum periplakin levels in patients with UCB than in normal controls ($p<0.0001$).

ROC curve analysis of serum periplakin level was performed for the comparison between the UCB group and the control group. The AUC-ROC level for UCB was 0.845 (95% CI=0.752-0.937) (Figure 2). The sensitivity and specificity in UCB, using a cut-off point of 4.045, were 83.7% (95% CI=70.3%-92.7%) and 73.3% (95% CI=54.1%-87.7%), respectively.

Association of preoperative serum periplakin with clinicopathological characteristics

The association of serum periplakin with clinicopathological features is shown in Table 1. Median serum periplakin levels in patients with NMIBC and MIBC were 0.00 and 1.48, respectively. Preoperative serum periplakin levels were significantly higher in patients with MIBC than in patients with NMIBC (p=0.03). There were no significant differences in serum periplakin levels in terms of gender, age, pathological grade, LVI, and lymph node status (p>0.05).

Association of periplakin expression with prognosis

Disease progression was observed in 13 patients (26%) (median time to progression=25.4; mean=27.4; range=4.8–64.8 months). Twelve patients (24%) (median time to death=29; mean=33.7; range= 9.2–80.4 months) died during the study period.

The Kaplan Meier method using the log-rank test indicated that the normalized signals from patients with serum periplakin above the median level of 0.31 showed no significant differences in terms of progression and cancer-specific survival.

In multivariate Cox proportional hazards regression analysis controlling for preoperative serum periplakin levels, pathological stage and grade, LVI, and lymph node status as dichotomous variables, none of the factors was associated with an increased risk for progression or cancer-specific survival.

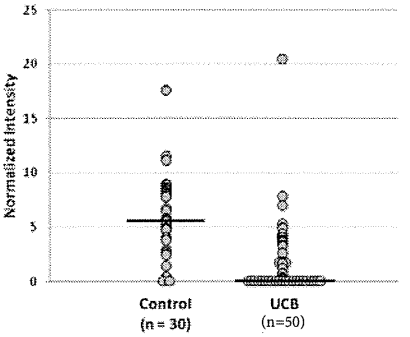

Figure 1. Serum Periplakin Expression Level in Normal Controls (n=30) and in those with Bladder Cancer (n=50) by Dot Blot Analysis. Horizontal lines indicate medians

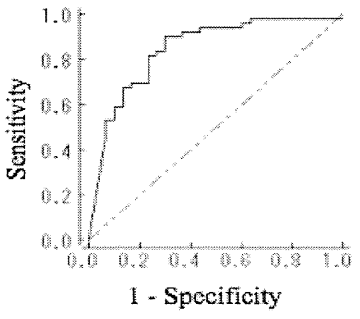

Figure 2. Receiver-Operating Characteristic (ROC) Analysis of Serum Periplakin Expression Level. The area under the curve-ROC level for bladder cancer was 0.845. The sensitivity and specificity, using a cut-off point of 4.045, were 83.7% and 73.3%, respectively

Table 1. Association of Preoperative Serum Periplakin Levels with Clinical and Pathological Characteristics

	Total no.of patients (%)	Serum periplakin levels Median	Mean	Range	P*
Gender					>0.99
Male	43 (86)	0.23	2.11	0.00-4.38	
Female	7 (14)	0.32	1.06	0.00-20.49	
Age (years)					0.41
<65	16 (32)	0	1.58	0.00-6.99	
≥65	34 (68)	0.51	2.14	0.00-20.49	
Pathological stage					0.03
pTa, pT1	27 (54)	0	1.15	0.00-4.08	
pT2, pT3, pT4	23 (46)	1.48	2.91	0.00-20.49	
Pathological grade					0.42
Grade 1, 2	26 (52)	0	1.7	0.00-7.88	
Grade 3	24 (48)	0.98	2.24	0.00-20.49	
LVI status					0.36
Negative	33 (67)	0.043	1.51	0.00-6.99	
Positive	17 (33)	0.74	2.85	0.00-20.49	
Lymph node status					0.44
Negative	44 (88)	0.5	2.12	0.00-3.75	
Positive	6 (12)	0.16	0.8	0.00-20.49	

*No: number; LVI: lymphovascular invasion. *Mann-Whitney U test

Discussion

UCB ranks in the top category of newly diagnosed cancers. High-risk disease of NMIBC revealed high rates (up to 90%) of recurrence (Shelley et al., 2010). It is important to diagnose UCB accurately and quickly with the help of a simple and cost-effective method. Although TUR and histological examination remain the gold standard, urine cytology is helpful as a noninvasive method of early diagnosis of UCB (Matsumoto et al., 2014). With the currently available modalities, there is no reliable biochemical or molecular examination that could be used as a universal screening tool for UCB.

Although investigations of autoantibodies to periplakin were performed in several reports (such as those involving pulmonary and skin diseases) (Park et al., 2006; Taille et al., 2011), this is the first study to evaluate serum periplakin for cancer detection, particularly UCB. Serum periplakin was significantly lower in patients with UCB than in normal controls. In addition, using the best cut-off point determined by the ROC curve, preoperative serum periplakin potentially acts as a biomarker for diagnosis. With encouraging results using the dot plot system in regard to serum periplakin, the diagnosis of UCB could become more simple and noninvasive.

Recent studies reported the biological role of periplakin in cancerous lesions. Downregulation of periplakin was correlated with the progression of esophageal squamous cell carcinoma (Hatakeyama et al., 2006; Nishimori et al., 2006). Cyclin A2–induced upregulation of periplakin was associated with poor prognosis as well as cisplatin resistance in endometrial cancer cells (Suzuki et al., 2010). Periplakin silencing reduced migration and attachment of pharyngeal squamous cancer cells (Tonoike et al., 2011). Periplakin silencing in triple-negative breast cancer cells